LNF-93/077 (P)

Low – Energy Photon – Photon Collisions to Two Loop Order

S. Bellucci, J. Gasser, M.E. Sainio

Nuclear Physics B 423, 80-122 (1994)

ELSEVIER

Nuclear Physics B 423 (1994) 80–122

NUCLEAR PHYSICS B

Low-energy photon–photon collisions to two-loop order ⋆

S. Bellucci [a], J. Gasser [b], M.E. Sainio [b,c,1]

[a] *INFN – Laboratori Nazionali di Frascati, P.O. Box 13, I-00044 Frascati, Italy*

[b] *Institute for Theoretical Physics, University of Bern, Sidlerstrasse 5, CH-3012 Bern, Switzerland*

[c] *Paul Scherrer Institut, CH-5232 Villigen PSI, Switzerland*

Received 17 January 1994; accepted 7 February 1994

Abstract

We evaluate the amplitude for $\gamma\gamma \to \pi^0\pi^0$ to two loops in chiral perturbation theory. The three new counterterms which enter at this order in the low-energy expansion are estimated with resonance saturation. We find that the cross section agrees rather well with the available data and with dispersion theoretic calculations even substantially above threshold. Numerical results for the Compton cross section and for the neutral pion polarizabilities are also given to two-loop accuracy.

1. Introduction

The cross section for $\gamma\gamma \to \pi^0\pi^0$ and for $\gamma\gamma \to \pi^+\pi^-$ has been calculated some time ago [1,2] in the framework of chiral perturbation theory (CHPT) [3–7] and of dispersion relations. For charged pion-pair production, the chiral calculation [1] at next-to-leading order is in good agreement with the Mark II data [8] in the low-energy region. On the other hand, for $\gamma\gamma \to \pi^0\pi^0$, the one-loop prediction [1,2] disagrees with the Crystal Ball data [9] and with dispersion theoretic calculations [10–16] even near threshold.

⋆ Work supported in part by Schweizerischer Nationalfonds and by the EEC Human Capital and Mobility Program.

[1] During the academic year 1992–93 on leave of absence from Department of Theoretical Physics, University of Helsinki, Helsinki, Finland.

SSDI 0550-3213(94)00070-U

In the process $\gamma\gamma \to \pi^+\pi^-$, the leading contribution[2] is generated by tree diagrams. One has a control on higher-order corrections in this case, in the sense that it is explicitly seen that the one-loop graphs do not modify the tree amplitude very strongly near threshold [1]. Tree diagrams are absent for $\gamma\gamma \to \pi^0\pi^0$ which starts out with one-loop graphs. It is the aim of this article to establish the region of validity of the chiral representation of this process by evaluating the amplitude at two-loop order.

Is a next-to-leading order calculation sufficient in this case? If the corrections are large, the reliability of the result is certainly doubtful. However, a glance at the data shows that the corrections needed to bring CHPT and experiment into agreement are not large – a 25–30% change in amplitude is sufficient. Corrections of this size are rather normal in reactions where pions in an isospin zero S-wave state are present [19]. As an example we mention the isospin zero S-wave $\pi\pi$ scattering length, whose tree-level value [20] receives a 25% correction from one-loop graphs [4]. Corrections of a similar size are present in the scalar form factor of the pion [21].

The amplitude for $\gamma\gamma \to \pi^0\pi^0$ also describes Compton scattering on neutral pions by analyticity and crossing. Do sizeable corrections in $\gamma\gamma \to \pi^0\pi^0$ then also show up in $\gamma\pi^0 \to \gamma\pi^0$? Since there are no strongly interacting particles in the final state in this case, one might be led to suspect that the one-loop amplitude is a good approximation for this reaction. We find it interesting that this is not the case – the corrections to the leading-order term are in fact very large in this channel.

The electromagnetic polarizabilities characterize aspects of the inner structure of hadrons. With the two-loop expression for the amplitude at hand, it is straightforward to evaluate the polarizabilities at next-to-leading order in the quark mass expansion. Renormalization group arguments show that this expansion contains logarithmic singularities of the type $M_\pi \ln^2 M_\pi^2$ and $M_\pi \ln M_\pi$, and an order of magnitude estimate reveals that these contributions may easily be as large as the leading-order term, unless the relevant Clebsch-Gordan coefficient is small. We find that the latter is the case.

Recently, a reformulation of CHPT has been given [22], where the effective lagrangian includes into each order additional terms which in the standard CHPT (considered here) are relegated to higher orders. To all orders, the two perturbative schemes are identical – in each finite order, they may, however, substantially differ. For an analysis of the process $\gamma\gamma \to \pi^0\pi^0$ in this generalized framework we refer the reader to Ref. [23].

The article is organized as follows. In sect. 2, we set up the notation. In sect. 3 we describe the low-energy expansion in a general manner and outline the specific procedure for the two-loop case in sects. 4 and 5. The low-energy constants which occur in the amplitude for $\gamma\gamma \to \pi^0\pi^0$ at two-loop order are determined in sect. 6. Sect. 7 contains a discussion of the amplitude and of the cross section at two-loop order. The Compton amplitude and the pion polarizabilities are described in sect. 8, whereas sect. 9 is devoted to a comparison of the chiral expansion with the dispersive analysis of $\gamma\gamma \to \pi^0\pi^0$ by Donoghue and Holstein [13]. Finally, a summary and concluding remarks are presented in sect. 10.

[2] In this article, we denote the first nonvanishing contribution to any quantity by "the leading-order term", independently of whether it starts out at tree level or at higher order in the chiral expansion.

2. Kinematics

The matrix element for pion production

$$\gamma(q_1)\gamma(q_2) \to \pi^0(p_1)\pi^0(p_2) \tag{2.1}$$

is given by

$$\langle \pi^0(p_1)\pi^0(p_2)\text{out} \mid \gamma(q_1)\gamma(q_2)\text{in}\rangle = i(2\pi)^4\delta^4(P_f - P_i)T^N\,, \tag{2.2}$$

with

$$T^N = e^2\epsilon_1^\mu\epsilon_2^\nu V_{\mu\nu}\,,$$
$$V_{\mu\nu} = i\int \mathrm{d}x\, \mathrm{e}^{-i(q_1x+q_2y)}\langle \pi^0(p_1)\pi^0(p_2)\text{out} \mid Tj_\mu(x)j_\nu(y) \mid 0\rangle. \tag{2.3}$$

Here j_μ is the electromagnetic current, and $\alpha = e^2/4\pi \simeq 1/137$. The decomposition of the correlator $V_{\mu\nu}$ into Lorentz invariant amplitudes reads with $q_1^2 = q_2^2 = 0$ (see Appendix A)

$$V_{\mu\nu} = A(s,t,u)T_{1\mu\nu} + B(s,t,u)T_{2\mu\nu} + C(s,t,u)T_{3\mu\nu} + D(s,t,u)T_{4\mu\nu}\,,$$
$$T_{1\mu\nu} = \tfrac{1}{2}sg_{\mu\nu} - q_{1\nu}q_{2\mu}\,,$$
$$T_{2\mu\nu} = 2s\Delta_\mu\Delta_\nu - \nu^2 g_{\mu\nu} - 2\nu(q_{1\nu}\Delta_\mu - q_{2\mu}\Delta_\nu)\,,$$
$$T_{3\mu\nu} = q_{1\mu}q_{2\nu}\,,$$
$$T_{4\mu\nu} = s(q_{1\mu}\Delta_\nu - q_{2\nu}\Delta_\mu) - \nu(q_{1\mu}q_{1\nu} + q_{2\mu}q_{2\nu})\,,$$
$$\Delta_\mu = (p_1 - p_2)_\mu\,, \tag{2.4}$$

where

$$s = (q_1 + q_2)^2\,, \qquad t = (p_1 - q_1)^2\,, \qquad u = (p_2 - q_1)^2\,,$$
$$\nu = t - u\,, \tag{2.5}$$

are the standard Mandelstam variables. The tensor $V_{\mu\nu}$ satisfies the Ward identities

$$q_1^\mu V_{\mu\nu} = q_2^\nu V_{\mu\nu} = 0\,. \tag{2.6}$$

The amplitudes A and B are analytic functions of the variables s, t and u, symmetric under crossing $(t,u) \to (u,t)$. The quantities C and D do not contribute to the process considered here (gauge invariance).

It is useful to introduce in addition the helicity amplitudes

$$H_{++} = A + 2(4M_\pi^2 - s)B\,,$$
$$H_{+-} = \frac{8(M_\pi^4 - tu)}{s}B\,. \tag{2.7}$$

The helicity components H_{++} and H_{+-} correspond to photon helicity differences $\lambda = 0, 2$, respectively. They have partial wave expansions involving even $J \geqslant \lambda$,

$$H_{++} = \sum_{J=0,2,4\ldots} h_+^J(s) d_{00}^J(\cos\theta) ,$$

$$H_{+-} = \sum_{J=2,4,6\ldots} h_-^J(s) d_{20}^J(\cos\theta) , \tag{2.8}$$

where θ is the scattering angle in the center-of-mass system, $q_1 \cdot p_1 = |q_1||p_1|\cos\theta$.

With our normalization of states $\langle p_1 \mid p_2\rangle = 2(2\pi)^3 p_1^0 \delta^3(p_1 - p_2)$, the differential cross section for unpolarized photons in the center-of-mass system is

$$\frac{d\sigma^{\gamma\gamma\to\pi^0\pi^0}}{d\Omega} = \frac{\alpha^2 s}{64}\beta(s)H(s,t) ,$$
$$H(s,t) = |H_{++}|^2 + |H_{+-}|^2 ,$$
$$\beta(s) = (1 - 4M_\pi^2/s)^{1/2} . \tag{2.9}$$

The amplitude for Compton scattering

$$\gamma(q_1)\pi^0(p_1) \to \gamma(q_2)\pi^0(p_2)$$

may be obtained by crossing. In the center-of-mass system, the cross section for unpolarized photons is

$$\frac{d\sigma^{\gamma\pi^0\to\gamma\pi^0}}{d\Omega} = \frac{\alpha^2}{16\bar{s}}\bar{t}^2 H(\bar{t},\bar{s}) , \tag{2.10}$$

with

$$\bar{s} = (q_1 + p_1)^2 , \qquad \bar{t} = (q_2 - q_1)^2 .$$

Finally, the optical theorem in the Compton channel reads with our phase convention

$$e^2 \operatorname{Im} B|_{s=0,t=\bar{s}} = \frac{1}{4(\bar{s} - M_\pi^2)}\sigma_{\text{tot}}^{\gamma\pi^0}(\bar{s}) . \tag{2.11}$$

This relation fixes the phase of A through Eq. (2.4).

The physical region for the reactions $\gamma\gamma \to \pi^0\pi^0$ and $\gamma\pi^0 \to \gamma\pi^0$ is displayed in Fig. 1, where we also indicate with shaded lines the nearest singularities in the amplitudes A and B. These singularities are generated by two-pion intermediate states in the s, t and u channel.

3. Low-energy expansion

We consider QCD with two flavours in the isospin symmetry limit $m_u = m_d = \hat{m}$ and equip the underlying lagrangian with hermitian, colour neutral external fields v, a, s and p in the standard manner,

$$\mathcal{L} = \mathcal{L}_{\text{QCD}}^0 + \bar{q}\gamma^\mu(v_\mu + a_\mu\gamma_5)q - \bar{q}(s - i\gamma_5 p)q . \tag{3.1}$$

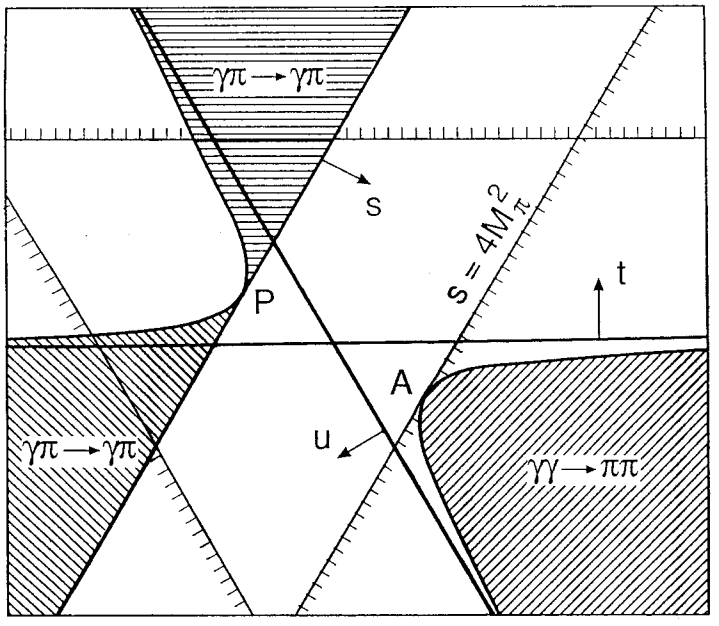

Fig. 1. Mandelstam plane showing the three related physical regions. s-channel: $\gamma\gamma \to \pi\pi$, t-and u-channel: $\gamma\pi \to \gamma\pi$. We indicate the threshold for $\gamma\gamma \to \pi\pi(\gamma\pi \to \gamma\pi)$ by A (P). The shaded lines at $s, t, u = 4M_\pi^2$ indicate the presence of a branch-point in the amplitude, generated by two-pion intermediate states.

Here $\mathcal{L}^0_{\rm QCD}$ denotes the QCD lagrangian at zero quark mass, whereas $\hat{m}$ is contained in the scalar field $s(x)$. The lagrangian (3.1) is invariant under local $SU(2)_L \times SU(2)_R \times U(1)$ transformations

$$q \to \tfrac{1}{2}[(1+\gamma_5)g_R + (1-\gamma_5)g_L]q \tag{3.2}$$

with

$$\begin{aligned} &g_{R,L} = \mathrm{e}^{i\phi}\, V_{R,L}\,, \\ &V_{R,L} \in SU(2)\,, \\ &\phi = \mathrm{diag}(\phi_0, \phi_0)\,, \quad \phi_0 \in \mathbb{R}\,, \end{aligned} \tag{3.3}$$

provided that the external fields are subject to the gauge transformation

$$\begin{aligned} r'_\mu &= g_R r_\mu g_R^\dagger + i g_R \partial_\mu g_R^\dagger\,, \\ l'_\mu &= g_L l_\mu g_L^\dagger + i g_L \partial_\mu g_L^\dagger\,, \\ s' + ip' &= g_R(s+ip)g_L^\dagger\,, \\ r_\mu &= v_\mu + a_\mu\,, \qquad l_\mu = v_\mu - a_\mu\,. \end{aligned} \tag{3.4}$$

Since the charge is not a generator of $SU(2)$, we consider in the following the case

$$\langle a_\mu \rangle = 0\,, \qquad \langle v_\mu \rangle \neq 0\,, \tag{3.5}$$

where $\langle A \rangle$ denotes the trace of the matrix A. The condition (3.5) is consistent with the transformation law (3.4). The Green functions of the theory are generated by the vacuum-to-vacuum amplitude

$$e^{iZ(v,a,s,p)} = \langle 0_{\text{out}} \mid 0_{\text{in}} \rangle_{v,a,s,p} . \tag{3.6}$$

The generating functional Z admits an expansion in powers of the external momenta and of the quark masses [3–5],

$$Z = Z_2 + Z_4 + Z_6 + \dots , \tag{3.7}$$

where Z_n denotes a term of order E^n. We write the corresponding expansion of the amplitudes as

$$I = I_2 + I_4 + I_6 + \dots , \qquad I = V^{\mu\nu}, A, B , \tag{3.8}$$

where it is understood that Z_n generates I_n [3]. To calculate $V^{\mu\nu}$, we set

$$s = \hat{m}\mathbf{1} , \qquad v_\mu = Q\bar{v}_\mu , \qquad p = \tau^3 \bar{p} , \qquad a_\mu = 0 , \tag{3.9}$$

where

$$Q = \tfrac{1}{3}\,\mathrm{diag}(2, -1) \tag{3.10}$$

is the charge matrix, and where $\bar{v}_\mu$ and $\bar{p}$ denote flavour neutral external fields. $V^{\mu\nu}$ is obtained from the term of order $\bar{v}^2\bar{p}^2$ in Z.

3.1. Terms at order E^2

In the meson sector, Z_2 is given by the classical action

$$Z_2 = \int \mathrm{d}x\, \mathcal{L}_2(U, v, a, s, p) , \tag{3.11}$$

where $\mathcal{L}_2$ is the nonlinear σ-model lagrangian

$$\mathcal{L}_2 = \tfrac{1}{4}F^2 \langle D_\mu U D^\mu U^\dagger + \chi^\dagger U + \chi U^\dagger \rangle , \tag{3.12}$$

evaluated at the solution to the classical equation of motion $\delta \int \mathcal{L}_2 = 0$. The 2×2 unitary matrix U contains the pion fields,

$$U = \sigma + i\frac{\phi}{F} , \qquad \sigma^2 + \frac{\phi^2}{F^2} = \mathbf{1} ,$$
$$\phi = \begin{pmatrix} \pi^0 & \sqrt{2}\pi^+ \\ \sqrt{2}\pi^- & -\pi^0 \end{pmatrix} = \phi^i \tau^i . \tag{3.13}$$

It transforms as

$$U \xrightarrow{G} g_R U g_L^\dagger \tag{3.14}$$

[3] Notice that I_n is not of order E^n.

under $G = SU(2)_L \times SU(2)_R \times U(1)$. The covariant derivative is

$$D_\mu U = \partial_\mu U - i r_\mu U + i U l_\mu , \tag{3.15}$$

and the field χ denotes the combination

$$\chi = 2B(s + ip). \tag{3.16}$$

F is the pion decay constant in the chiral limit, $F_\pi = F(1 + O(\hat{m}))$, $F_\pi \simeq 93$ MeV, and B is related to the order parameter $\langle 0 \mid \bar{q}q \mid 0 \rangle$. The physical pion mass is

$$\begin{aligned} M_\pi^2 &= M^2(1 + O(\hat{m})) , \\ M^2 &= 2\hat{m}B. \end{aligned} \tag{3.17}$$

$\mathcal{L}_2$ is referred to as the effective lagrangian at order E^2.

The term of order $O(\bar{v}^2\bar{p}^2)$ in the classical action Z_2 vanishes and, therefore, one has

$$A_2 = B_2 = V_2^{\mu\nu} = 0 . \tag{3.18}$$

3.2. Higher orders in the energy expansion

At higher orders in the energy expansion, the effective lagrangian consists of a string of terms. Re-introducing momentarily $\hbar$, one has

$$\mathcal{L}_{\text{eff}} = \mathcal{L}_2 + \hbar\mathcal{L}_4 + \hbar^2\mathcal{L}_6 + \dots . \tag{3.19}$$

Here $\mathcal{L}_4$ contains all possible contributions with four derivatives, or two derivatives and one field χ, or χ^2, and similarly for the higher-order terms ($\mathcal{L}_4$ contains in addition the Wess–Zumino–Witten lagrangian $\mathcal{L}_{\text{WZW}}$ [24]). The generating functional is given by

$$\exp\left(\frac{i}{\hbar} Z(v,a,s,p)\right) = \int [\, \mathrm{d}U] \exp\left(\frac{i}{\hbar} \int \mathcal{L}_{\text{eff}}\, \mathrm{d}x\right) , \tag{3.20}$$

and its low-energy expansion is obtained from $Z = Z_2 + \hbar Z_4 + \dots$. One expands

$$\mathcal{L}_I = \bar{\mathcal{L}}_I + C_I\xi + \tfrac{1}{2}\xi D_I \xi + E_I\xi^3 + F_I\xi^4 + \dots , \qquad I = 2,4,\dots , \tag{3.21}$$

where $\bar{\mathcal{L}}_I$ denotes the lagrangian $\mathcal{L}_I$, evaluated at the solution to the classical equation of motion $\delta \int \mathcal{L}_2 = 0$. (To simplify the notation, we have dropped the $SU(2)$ indices in ξ and in the operators C_I, D_I, ...) The fluctuation ξ is of order $\hbar^{1/2}$. Then one obtains

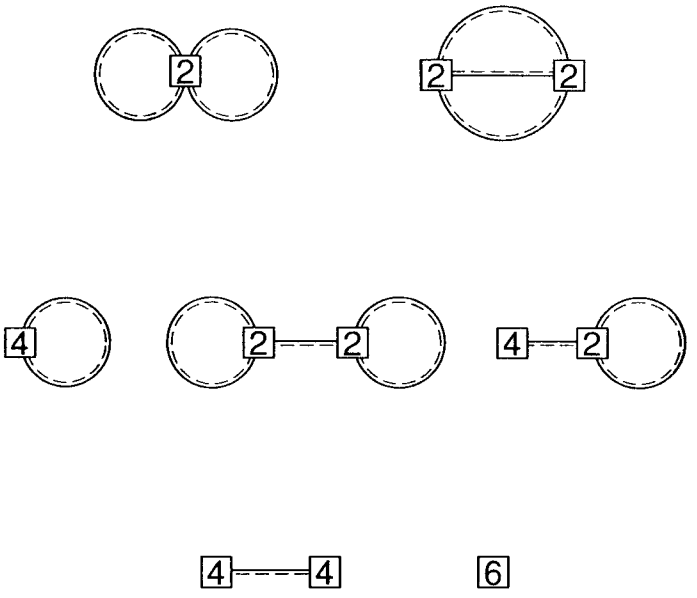

Fig. 2. The graphs at order E^6 in the chiral expansion. These graphs correspond to the terms in Eq. (3.22). The framed symbols I stand for the vertices in $\mathcal{L}_I$. We indicate with the solid-dashed lines the propagator D_2^{-1}.

$$\exp\left(\frac{iZ}{\hbar}\right) = \exp\left(\frac{i}{\hbar} S_{\rm cl}\right) \int [\,\mathrm{d}\xi]\, \exp\left(\frac{i}{\hbar} \int \tfrac{1}{2}\xi D_2 \xi \,\mathrm{d}x\right) \triangle ,$$

$$\triangle = 1 - \frac{1}{2\hbar^2} \int \left[(E_2\xi^3 + \hbar C_4\xi)_x (E_2\xi^3 + \hbar C_4\xi)_y\right] \mathrm{d}x\, \mathrm{d}y$$

$$+ \frac{i}{2\hbar} \int \left[2F_2\xi^4 + \hbar\xi D_4 \xi\right]_x \mathrm{d}x + O(\hbar^2) , \qquad (3.22)$$

with $S_{\rm cl} = \int \mathrm{d}x\, \bar{\mathcal{L}}_{\rm eff}$.

At order E^4, this result amounts to evaluating one-loop graphs generated by $\mathcal{L}_2$ and adding the tree graphs from $\mathcal{L}_2 + \hbar\mathcal{L}_4$ [4]. These contributions then add up to Z_4, which contains the leading-order term $V_4^{\mu\nu}$. It is a specific feature of the process $\gamma\gamma \to \pi^0\pi^0$ that the counterterms contained in $\mathcal{L}_4$ do not contribute to $V_4^{\mu\nu}$–the sum of the one-loop graphs is therefore ultraviolet finite [1,2].

The diagrams which generate Z_6 are displayed in Fig. 2. The solid-dashed lines stand for the propagator D_2^{-1}, and the framed symbols I denote vertices from $\mathcal{L}_I$ according to Eq. (3.21).

In order not to interrupt the argument, we relegate the discussion of the leading contribution $V_4^{\mu\nu}$ to Appendix B and continue in the following section with the evaluation of the next-to-leading order term $V_6^{\mu\nu}$.

4. Renormalization

The evaluation of $V_6^{\mu\nu}$ is complex. We outline in this and in the following two sections the procedure – omitting, however, all details.

4.1. The lagrangians $\mathcal{L}_4$ and $\mathcal{L}_6$

The lagrangian $\mathcal{L}_4$ contributes to $V_6^{\mu\nu}$ through one-loop diagrams, see Fig. 2. Its general form is [4]

$$\begin{aligned}\mathcal{L}_4 &= \mathcal{L}^{(4)} + \mathcal{L}_{\mathrm{WZW}}\,,\\ \mathcal{L}^{(4)} &= \sum_{i=1}^{7} l_i P_i + \dots\,,\end{aligned} \tag{4.1}$$

where

$$\begin{aligned}P_1 &= \tfrac{1}{4}\langle u^\mu u_\mu\rangle^2\,,\\ P_2 &= \tfrac{1}{4}\langle u_\mu u_\nu\rangle\langle u^\mu u^\nu\rangle\,,\\ P_3 &= \tfrac{1}{16}\langle \chi_+\rangle^2\,,\\ P_4 &= \tfrac{1}{4}i\langle u_\mu \chi_-^\mu\rangle\,,\\ P_5 &= -\tfrac{1}{2}\langle f_-^{\mu\nu} f_{-\mu\nu}\rangle\,,\\ P_6 &= \tfrac{1}{4}i\langle f_+^{\mu\nu}[u_\mu, u_\nu]\rangle\,,\\ P_7 &= -\tfrac{1}{16}\langle \chi_-\rangle^2.\end{aligned} \tag{4.2}$$

Here we used the notation

$$\begin{aligned}u_\mu &= iu^\dagger D_\mu U u^\dagger = -iuD_\mu U^\dagger u = u_\mu^\dagger\,,\\ \chi_\pm &= u^\dagger \chi u^\dagger \pm u\chi^\dagger u\,,\\ \chi_-^\mu &= u^\dagger D^\mu \chi u^\dagger - uD^\mu \chi^\dagger u\,,\\ f_\pm^{\mu\nu} &= uF_L^{\mu\nu}u^\dagger \pm u^\dagger F_R^{\mu\nu} u\,,\end{aligned} \tag{4.3}$$

with $u^2 = U$. The quantity $F_R^{\mu\nu}$ ($F_L^{\mu\nu}$) stands for the field strength associated with the nonabelian external field $v_\mu + a_\mu$ ($v_\mu - a_\mu$).

The ellipsis in (4.1) denotes polynomials in the external fields which are independent of the pion variables. These do not contribute to S-matrix elements and are therefore not needed in the following. Finally, the anomaly term $\mathcal{L}_{\mathrm{WZW}}$ contributes to $V_8^{\mu\nu}$ [25]. This is beyond the accuracy of the low-energy expansion considered here.

The realization of G on u is

$$u \xrightarrow{G} g_R u h^\dagger = h u g_L^\dagger\,, \tag{4.4}$$

such that

$$I \xrightarrow{G} hIh^\dagger \tag{4.5}$$

for the quantities in (4.3). The low-energy constants l_i are divergent, except l_7. They remove the ultraviolet divergences generated by the one-loop graphs – we discuss them in more detail below.

In the construction of $\mathcal{L}^{(4)}$, the equation of motion $\delta \int \mathcal{L}_2 = 0$ has been used. It can be shown that adding terms to $\mathcal{L}^{(4)}$ which vanish upon use of the equation of motion affects the generating functional at order E^6 by a local term[4] – these contributions may thus be omitted.

The lagrangian $\mathcal{L}_6$ contributes a polynomial part to $V_6^{\mu\nu}$ which cancels the ultraviolet singularities generated by the two-loop diagrams. The general structure of $\mathcal{L}_6$ is not yet available in the literature [26]. Concerning the present calculation, we note that the lagrangian

$$\begin{aligned}
\mathcal{L}_6 &= \frac{1}{F^2}\langle f_{+\mu\rho} f_+^{\mu\sigma} + f_{-\mu\rho} f_-^{\mu\sigma}\rangle T_\sigma^\rho + \dots , \\
T_{\rho\sigma} &= d_1\langle u_\rho u_\sigma\rangle + g_{\rho\sigma}\{d_2\langle u^\mu u_\mu\rangle + d_3\langle\chi_+\rangle\}
\end{aligned} \tag{4.6}$$

generates a polynomial in A_6, B_6 which has the same structure as the divergent part in the two-loop contribution,

$$\begin{aligned}
A_6 &= \frac{20}{9F^4}\,[16(d_3 - d_2)M^2 + (d_1 + 8d_2)s] + \dots , \\
B_6 &= -\frac{10}{9F^4}\,d_1 + \dots .
\end{aligned} \tag{4.7}$$

We may therefore remove the divergences in $V_6^{\mu\nu}$ by simply dropping the singular parts in A_6 and B_6, see below.

4.2. Regularization and renormalization

We use dimensional regularization and set

$$\omega = d - 4 , \tag{4.8}$$

where d is the dimension of space-time. We introduce the renormalization scale μ such that the calculation is scale-independent at each step. In the following we outline the procedure [27].

Consider the couplings l_i in $\mathcal{L}^{(4)}$ which carry dimension $(\text{mass})^\omega$. We treat l_i as μ-independent parameters by writing in the minimal subtraction scheme

$$l_i = \mu^\omega \left\{ \frac{\delta_i}{\omega} + l_i^{\text{MS}} + \omega l_{i1}^{\text{MS}} + O(\omega^2) \right\} , \qquad i = 1, \dots , 7 , \tag{4.9}$$

[4] We thank G. Ecker for an explicit proof of this statement and for illuminating discussions concerning the material in subsect. 4.2.

with

$$\mu\frac{\mathrm{d}l_i^{\mathrm{MS}}}{\mathrm{d}\mu} = -\delta_i\,, \qquad \mu\frac{\mathrm{d}l_{i1}^{\mathrm{MS}}}{\mathrm{d}\mu} = -l_i^{\mathrm{MS}}\,. \tag{4.10}$$

The divergent terms δ_i/ω remove the one-loop singularities in Z_4 (the δ_i are related to the γ_i used in Ref. [4] by $\delta_i = \gamma_i/16\pi^2$). Since the l_i occur in Z_6 via loop insertions, the constants l_{i1}^{MS} in general also contribute at two-loop order. For an illustration of the renormalization procedure, we consider the amplitude F^4B which has dimension $(\mathrm{mass})^{2\omega}$. We write for the contribution from the loops

$$B = \frac{\mu^{2\omega}}{F^4}\left\{\text{Laurent-series of } (\mu^{-2\omega}F^4B) \text{ at } \omega = 0\right\}\,. \tag{4.11}$$

From $\mathcal{L}^{(4)}$, only l_2 contributes,

$$B = \frac{1}{F^4}\left\{M^{2\omega}f(s/M^2,t/M^2;\omega) + M^{\omega}l_2\, g(s/M^2,t/M^2;\omega)\right\}\,, \tag{4.12}$$

where f and g are singular as $\omega \to 0$,

$$\begin{aligned} f &= \frac{f_2}{\omega^2} + \frac{f_1}{\omega} + f_0 + O(\omega)\,,\\ g &= \frac{g_1}{\omega} + g_0 + \omega g_{+1} + O(\omega^2)\,. \end{aligned} \tag{4.13}$$

The Laurent-series (4.11) becomes

$$B = \frac{\mu^{2\omega}}{F^4}\left\{\frac{\beta_2}{\omega^2} + \frac{\beta_1 l_2^{\mathrm{MS}} + \beta_{1,1}}{\omega} + \beta^{\mathrm{MS}} + O(\omega)\right\}\,. \tag{4.14}$$

The residues of the pole terms are

$$\beta_2 = \frac{\delta_2 g_1}{2}\,, \qquad \beta_1 = g_1\,, \qquad \beta_{1,1} = \delta_2 g_0 + f_1\,, \tag{4.15}$$

and for the finite part we find

$$\beta^{\mathrm{MS}} = \frac{g_1}{8}\left\{-\delta_2 \ln\frac{M^2}{\mu^2} + 4l_2^{\mathrm{MS}}\right\}\ln\frac{M^2}{\mu^2} + c_1 \ln\frac{M^2}{\mu^2} + c_2\,. \tag{4.16}$$

Here the c_i stand for linear combinations of $f_1,\ldots,g_{+1}$.

Without having evaluated any Feynman diagram, we have already obtained significant information on the structure of the two-loop result [3]:

(i) The residues of the pole-terms in (4.14) are polynomials in the external momenta and in the masses on general grounds [28]. For dimensional reasons, these polynomials reduce to pure numbers in the present case. In addition, from the cancellation of the logarithmic terms which are generated by expanding the factors $M^{2\omega}$ and M^{ω} in (4.12), it follows that the residue of the double pole in f is proportional to the residue of the single pole in g,

$$2f_2 + \delta_2 g_1 = 0\,, \tag{4.17}$$

or

$$2\beta_2 = \delta_2\beta_1 \,. \tag{4.18}$$

(ii) The amplitude f contains a nonlocal singularity f_1/ω which is generated by divergent subgraphs. This nonlocality must be cancelled by the nonlocal singular part $\delta_2 g_0/\omega$ in the graphs generated by loops with $\mathcal{L}^{(4)}$, in such a way that $\beta_{1,1} = \delta_2 g_0 + f_1$ becomes a pure number.

(iii) As is seen from Eq. (4.16), the finite part $\beta^{\rm MS}$ contains chiral logarithms $\ln^2 M^2$ and $\ln M^2$. The coefficient of the leading term $\ln^2 M^2$ is proportional to the residue of the single pole in g, whereas the linear piece $\ln M^2$ is multiplied with a nonlocal function. These singular terms cancel the chiral logarithms in c_2 and thus generate a smooth behaviour of the amplitude in the chiral limit $\hat{m} \to 0$ (at fixed $s, t \neq 0$).

(iv) At the Compton threshold $s = 0, t = M^2$, the quantities c_1 and c_2 are independent of the quark mass. Therefore, the chiral logarithms $\ln^2 M^2$ and $\ln M^2$ in Eq. (4.16) remain, and we conclude that the finite part $\beta^{\rm MS}|_{s=0,t=M^2}$ blows up in the chiral limit. In other words, the slope of the form factor $V_9 = 2sB$ (see Appendix A) is infrared singular,

$$F^4 \frac{\mathrm{d}V_9}{\mathrm{d}s}\bigg|_{s=0,t=M^2} = \frac{g_1}{4}\left\{-\delta_2 \ln\frac{M^2}{\mu^2} + 4l_2^{\rm MS}\right\}\ln\frac{M^2}{\mu^2} + \bar{c}_1 \ln\frac{M^2}{\mu^2} + \bar{c}_2 \,, \tag{4.19}$$

where the $\bar{c}_i$ are independent of the quark mass. Notice that $\ln^2 M^2$ occurs together with $l_2^{\rm MS} \ln M^2$ in a particular combination which is dictated by Eq. (4.17).

We now define the renormalized amplitude $B^{\rm ren}$ as

$$B^{\rm ren} = \frac{1}{F^4}\left(\beta^{\rm MS} + b^{\rm MS}\right), \tag{4.20}$$

where the scale-dependence of $b^{\rm MS}$ is chosen such that $B^{\rm ren}$ is independent of μ,

$$\mu\frac{\mathrm{d}}{\mathrm{d}\mu} B^{\rm ren} = 0 \,. \tag{4.21}$$

(The low-energy parameter $b^{\rm MS}$ is the sum of the finite pieces of the relevant counterterms at order E^6 in the effective action.)

We have formulated the renormalization procedure in the minimal subtraction scheme, where $\ln(4\pi)$ and $\Gamma'(1)$ occur. One may eliminate these terms in the standard manner [29]. Below we use the conventions of Ref. [4]. The final result for B_6 contains one unknown new parameter b^r,

$$B_6 = \frac{b^r}{(16\pi^2F^2)^2} + \ldots \,. \tag{4.22}$$

Analogously, the renormalized amplitude A_6 contains two unknown new parameters a_1^r and a_2^r,

$$A_6 = \frac{a_1^r M^2 + a_2^r s}{(16\pi^2F^2)^2} + \ldots \,. \tag{4.23}$$

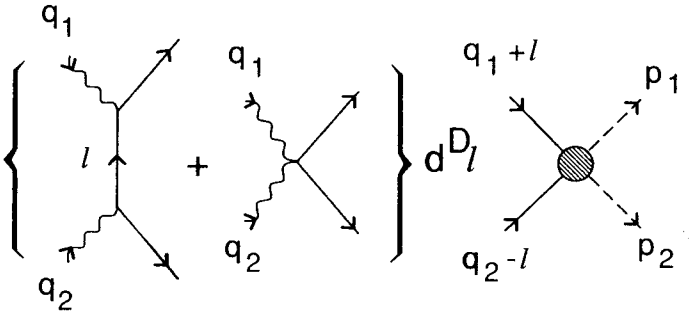

Fig. 3. One class of Feynman diagrams which contribute to $\gamma\gamma \to \pi^0\pi^0$. The dashed (solid) lines stand for neutral (charged) pions. The four-point function on the right-hand side is the elastic $\pi\pi$ scattering amplitude at one-loop accuracy in d dimensions (with two legs off-shell), and the symbol $\mathrm{d}^D l$ stands for integration over internal lines with weight (5.1).

The ellipses in (4.22) and (4.23) stand for the finite contributions from the loop-integrals.

5. Evaluation of diagrams

Here we discuss further aspects of the two-loop calculation.

5.1. The diagrams

It is straightforward to generate from Fig. 2 the diagrams for $\gamma\gamma \to \pi^0\pi^0$ at two-loop order – one has simply to insert photon and pion vertices in all possible ways. For illustration, we display one class of graphs in Fig. 3. The solid (dashed) line denotes charged (neutral) pions. The four-point function on the right-hand side is the d-dimensional elastic $\pi\pi$ scattering amplitude at one-loop accuracy, with two pions off-shell (the one-loop graphs for $\gamma\gamma \to \pi^0\pi^0$ are thus also included in Fig. 3). The symbol $\mathrm{d}^D l$ stands for integration over internal momenta with weight

$$\frac{1}{[M_\pi^2 - (l+q_1)^2][M_\pi^2 - (q_2 - l)^2]}\,, \tag{5.1}$$

where M_π^2 denotes the physical pion mass in one-loop approximation,

$$M_\pi^2 = M^2\left[1 + \frac{M^2}{F^2}\left(2l_3^r + \frac{1}{32\pi^2}\ln\frac{M^2}{\mu^2}\right) + O(M^4)\right]. \tag{5.2}$$

The momenta of the charged pions running in the loop are $(l+q_1)^\mu$ and $(q_2 - l)^\mu$. We do not display the remaining diagrams.

5.2. Numerical evaluation of diagrams

The derivative nature of the interaction makes the algebraic part of the calculation tedious. As for the numerical part, we have to evaluate the amplitudes in the physical

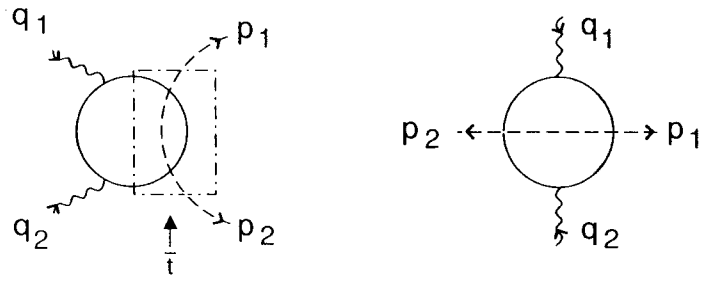

Fig. 4. Graphs which contribute to $\Delta_{A,B}$ in the unitary part $U_{A,B}$ in Eqs. (7.3), (7.8). In Fig. 4a, the dash-dotted lines surround the diagram which we represent in the dispersive manner (5.3). The graph Fig. 4b is called "acnode graph" [55].

region for $\gamma\gamma \to \pi^0\pi^0$ where branch-points and cuts appear. These render the numerical evaluation of the Feynman integrals nontrivial. To illustrate our procedure to cope with this difficulty, we consider the two-loop box diagram Fig. 4a. We write for the subdiagram (enclosed by dash-dotted lines) a d-dimensional spectral representation

$$J(\bar{t},d) = \int_{4M_\pi^2}^{\infty} \frac{\mathrm{d}\sigma\rho(\sigma,d)}{\sigma - \bar{t}}\,, \tag{5.3}$$

where $\bar{t}$ contains loop-momenta. This leads to a spectral representation for the full diagram,

$$\int_{4M_\pi^2}^{\infty} \mathrm{d}\sigma\rho(\sigma,d)b(s,t,\sigma,d), \tag{5.4}$$

where $b(s,t,\sigma,d)$ denotes a one-loop d-dimensional box diagram (one of the internal lines carries mass $\sqrt{\sigma}$). After removing the subdivergence generated by $J(\bar{t},d)$, we obtain the finite part by writing a fixed-t dispersion relation. This procedure allows one to evaluate numerically the amplitude also in the region $s > 4M_\pi^2$, $t < 9M_\pi^2$.

5.3. Checks on the calculation

As is shown in Appendix A, the most general expression for the amplitude $\epsilon_1^\mu \epsilon_2^\nu V_{\mu\nu}$ contains five form factors which are linearly related through two Ward identities and through Bose symmetry,

$$\begin{aligned} L_1(V_i) &\doteq 2V_0 + sV_4 - (t-u)V_5 = 0\,, \\ L_2(V_i) &\doteq \quad sV_7 - (t-u)V_9 = 0\,, \\ L_3(V_i) &\doteq \quad\quad V_5 + V_7 = 0\,. \end{aligned} \tag{5.5}$$

The amplitudes A and B may be obtained from V_4 and V_9,

$$A = -V_4\,, \qquad B = V_9/2s\,. \tag{5.6}$$

To get an optimal control of the calculation, we have fully evaluated all five form factors in d dimensions and have made the following consistency checks of the results:

(i) We have verified that the relations (5.5) are satisfied numerically within machine accuracy in low dimensions (below threshold).

(ii) We have determined the divergence structure at $\omega \to 0$,

$$V_i = \mu^{2\omega} \left\{ \frac{P_i^{(2)}}{\omega^2} + \frac{P_i^{(1)}}{\omega} + R_i + O(\omega) \right\}, \tag{5.7}$$

and have verified that the residues $P_i^{(k)}$ are polynomials in the external momenta and in the masses. These polynomials obey Eq. (5.5) as well,

$$L_m(P_i^{(k)}) = 0, \qquad m = 1,2,3, \qquad k = 1,2, \tag{5.8}$$

and are related in the manner discussed in the previous section, see Eq. (4.18) for $P_9^{(1)}$ and $P_9^{(2)}$.

(iii) We have checked that also the finite parts R_i satisfy numerically

$$L_m(R_i) = 0, \qquad m = 1,2,3 \tag{5.9}$$

within machine accuracy below threshold.

At this stage, we have written fixed-t dispersion relations for some of the finite parts in the manner mentioned above. This allows one to evaluate the complete amplitude in the physical region for pion-pair production.

(iv) We have then worked out the S-wave projection $h_+^0(s)$ (2.8) and have verified numerically that this amplitude has the correct phase at $s > 4M_\pi^2$, given by the (tree plus one-loop) elastic $\pi\pi$ scattering S-wave phase shift (in the appropriate isospin decomposition).

In addition, we have made many other cross-checks.

6. Low-energy constants at order E^6

Once the program described above is carried through, one ends up with ultraviolet finite and scale-independent amplitudes A and B which contain the parameters F, M_π; l_i^r, l_{i1}^r $(i = 1,2,3,5,6)$; a_1^r, a_2^r and b^r. F is related to the physical pion decay constant F_π [4],

$$F_\pi = F\left[1 + \frac{M^2}{F^2}\left(l_4^r - \frac{1}{16\pi^2}\ln\frac{M^2}{\mu^2}\right) + O(M^4)\right]. \tag{6.1}$$

We may therefore replace F by F_π at the expense of introducing l_4^r. The expressions for the loop-amplitudes simplify if one uses [4] the scale-independent parameters $\bar{l}_i$,

$$l_i^r = \frac{\delta_i}{2}\left(\bar{l}_i + \ln\frac{M^2}{\mu^2}\right). \tag{6.2}$$

Table 1
Phenomenological values [4,31] and source for the renormalized coupling constants $\bar{l}_i, i = 1,\ldots,6$. The quantities δ_i in the fourth column determine the scale dependence of the $l_i^r(\mu)$ according to Eq. (6.2). In the text we also use $\bar{l}_\Delta = \bar{l}_6 - \bar{l}_5$, see Eq. (6.3).

i	$\bar{l}_i$	Source	$16\pi^2\delta_i$
1	-0.8 ± 1.2	$K_{e4}, \pi\pi \to \pi\pi$	1/3
2	5.8 ± 0.7	$K_{e4}, \pi\pi \to \pi\pi$	2/3
3	2.9 ± 2.4	SU(3) mass formulae	−1/2
4	4.3 ± 0.9	F_K/F_π	2
5	13.8 ± 1.3	$\pi \to e\nu\gamma$	−1/6
6	16.5 ± 1.1	$\langle r^2\rangle_V^\pi$	−1/3

Table 2
Resonance contributions to the coupling constants a_1^r, a_2^r and b^r. Column 6 contains the sums of those contributions which have a definite sign. The calculation is presented in Appendix D.

	I^R					I^R	
I^r	ω	ρ^0	ϕ	$A(1^{+-})$	$\sum_R I^R$	$S(0^{++})$	f_2
a_1^r	−33.2	−6.1	−0.1	0.0	−39	±0.8	∓4.1
a_2^r	12.5	2.3	$\simeq 0$	−1.3	13	±1.3	±1.0
b^r	2.1	0.4	$\simeq 0$	0.7	3	0.0	±0.5

Their values are displayed in column 2 of Table 1. We note that $\bar{l}_5$ and $\bar{l}_6$ in the present application always appear in the combination

$$\bar{l}_\Delta = \bar{l}_6 - \bar{l}_5 = 2.7\,. \tag{6.3}$$

[The constant $\bar{l}_\Delta$ is related to the low-energy couplings L_9^r and L_{10}^r which occur in the $SU(3)_L \times SU(3)_R$ version of the one-loop amplitude $\gamma\gamma \to \pi^+\pi^-$ [1] by $\bar{l}_\Delta = 192\pi^2(L_9^r + L_{10}^r)$.] Next we observe that we may absorb l_{i1}^r's into the low-energy constants at order E^6, because they contribute a polynomial piece only. We are therefore left with a_1^r, a_2^r and b^r as the only new unknowns. We estimate these in the standard manner [4,30], replacing them at a scale $\mu = 500$ MeV ... 1 GeV by the contribution from resonance exchange. Let

$$I^r(\mu) = \sum_R I^R + \hat{I}^r(\mu)\,, \qquad I = a_1, a_2, b\,, \tag{6.4}$$

where the sum denotes contributions from scalar, (axial-)vector and tensor exchange. Our estimate for $I^r(M_\rho)$ consists in setting $\hat{I}^r(M_\rho) = 0$.

The quantities I^R are evaluated in Appendix D. The results of the calculation are displayed in Table 2, where the individual resonance contributions I^R are listed. Column 6 contains the sums of those contributions which have a definite sign.

To estimate the effects of the systematic uncertainties in the values of these couplings, it is useful to furthermore consider the helicity amplitudes H_{++} and H_{+-} and the corresponding low-energy constants $h_\pm^r$ and h_s^r,

$$H_{++}^{2\text{loops}} = \frac{1}{(16\pi^2F^2)^2}\left\{h_+^r M^2 + h_s^r\, s\right\} + \dots ,$$

$$H_{+-}^{2\text{loops}} = \frac{8(M^4 - tu)}{s(16\pi^2F^2)^2}\, h_-^r + \dots ,$$

$$h_+^r = a_1^r + 8b^r , \qquad h_s^r = a_2^r - 2b^r , \qquad h_-^r = b^r . \tag{6.5}$$

From column 6 in Table 2 we obtain the central values of these couplings. According to experience with resonance saturation at order E^4, we associate a 30% uncertainty to the contributions generated by (axial-)vector exchange and a 100% error to the contributions from scalars and from f_2. Adding these errors in quadrature, we find

$$h_+^r(M_\rho) = -14 \pm 5 ,$$
$$h_s^r(M_\rho) = 7 \pm 3 ,$$
$$h_-^r(M_\rho) = 3 \pm 1 . \tag{6.6}$$

Notice that tensor exchange does contribute neither to h_+^r nor to h_s^r, because the coupling (D.8) is purely D-wave. Scalars do not affect h_-^r.

In Ref. [35], these couplings have been determined (i) from vector-meson exchange and using nonet-symmetry, and (ii) from the chiral quark model, with the result

$$(h_+^r, h_s^r, h_-^r)|_{\mu=M_\rho} = \begin{cases} (-18, 9, 2) & \text{vector-mesons (nonet)}, \\ (-12, 6, 2) & \text{chiral quark model}, \end{cases} \tag{6.7}$$

which agrees within the uncertainties with the values in (6.6).

This completes the determination of the parameters which occur at two-loop order in $\gamma\gamma \to \pi^0\pi^0$.

7. Amplitudes and cross section to two loops

7.1. The amplitudes: analytic results

We obtain the following expression for the amplitude A to two loops:

$$A = A_4 + A_6 + O(E^4) , \tag{7.1}$$

or

$$A = \frac{4\bar{G}_\pi(s)}{sF_\pi^2}\,(s - M_\pi^2) + U_A + P_A + O(E^4). \tag{7.2}$$

The unitary part U_A contains s, t and u-channel cuts, and P_A is a linear polynomial in s. Explicitly,

$$U_A = \frac{2}{sF_\pi^4}\bar{G}(s)\left[(s^2 - M_\pi^4)\bar{J}(s) + C(s,\bar{l}_i)\right] + \frac{\bar{l}_\Delta}{24\pi^2 F_\pi^4}(s - M_\pi^2)\bar{J}(s)$$
$$+ \frac{(\bar{l}_2 - 5/6)}{144\pi^2 s F_\pi^4}(s - 4M_\pi^2)\{\bar{H}(s) + 4[s\bar{G}(s) + 2M_\pi^2(\bar{\bar{G}}(s) - 3\,\bar{\bar{J}}(s))]d_{00}^2\}$$
$$+ \Delta_A(s,t,u)\,, \tag{7.3}$$

with

$$C(s,\bar{l}_i) = \frac{1}{48\pi^2}\left\{2(\bar{l}_1 - \tfrac{4}{3})(s - 2M_\pi^2)^2 + \tfrac{1}{3}(\bar{l}_2 - \tfrac{5}{6})(4s^2 - 8sM_\pi^2 + 16M_\pi^4)\right.$$
$$\left. -3M_\pi^4\bar{l}_3 + 12M_\pi^2(s - M_\pi^2)\bar{l}_4 - 12sM_\pi^2 + 15M_\pi^4\right\}\,,$$
$$d_{00}^2 = \tfrac{1}{2}(3\cos\theta^2 - 1)\,. \tag{7.4}$$

The loop-functions $\bar{J}$, etc. are displayed in Appendix C. The quantity $\bar{G}_\pi(s)$ in Eq. (7.2) stands for $\bar{G}(s)$, evaluated with the physical pion mass, and θ denotes the scattering angle in the center-of-mass system. The term proportional to d_{00}^2 in U_A contributes to D-waves only. For Δ_A see below.

The polynomial part is

$$P_A = \frac{1}{(16\pi^2 F_\pi^2)^2}\left[a_1 M_\pi^2 + a_2 s\right]\,,$$
$$a_1 = a_1^r + \tfrac{1}{18}\left\{4l^2 + l(8\bar{l}_2 + 12\bar{l}_\Delta - \tfrac{4}{3}) - \tfrac{20}{3}\bar{l}_2 + 12\bar{l}_\Delta + \tfrac{110}{9}\right\}\,,$$
$$a_2 = a_2^r - \tfrac{1}{18}\left\{l^2 + l(2\bar{l}_2 + 12\bar{l}_\Delta + \tfrac{2}{3}) - \tfrac{5}{3}\bar{l}_2 + 12\bar{l}_\Delta + \tfrac{697}{144}\right\}\,,$$
$$l = \ln\frac{M^2}{\mu^2}\,. \tag{7.5}$$

The result for B is

$$B = B_6 + O(E^2)\,, \tag{7.6}$$

or

$$B = U_B + P_B + O(E^2)\,, \tag{7.7}$$

with unitary part

$$U_B = \frac{(\bar{l}_2 - \frac{5}{6})\bar{H}(s)}{288\pi^2 F_\pi^4 s} + \Delta_B(s,t,u)\,. \tag{7.8}$$

For the polynomial we obtain

$$P_B = \frac{b}{(16\pi^2 F_\pi^2)^2}\,,$$
$$b = b^r - \tfrac{1}{36}\left[l^2 + l(2\bar{l}_2 + \tfrac{2}{3}) - \tfrac{1}{3}\bar{l}_2 + \tfrac{393}{144}\right]\,. \tag{7.9}$$

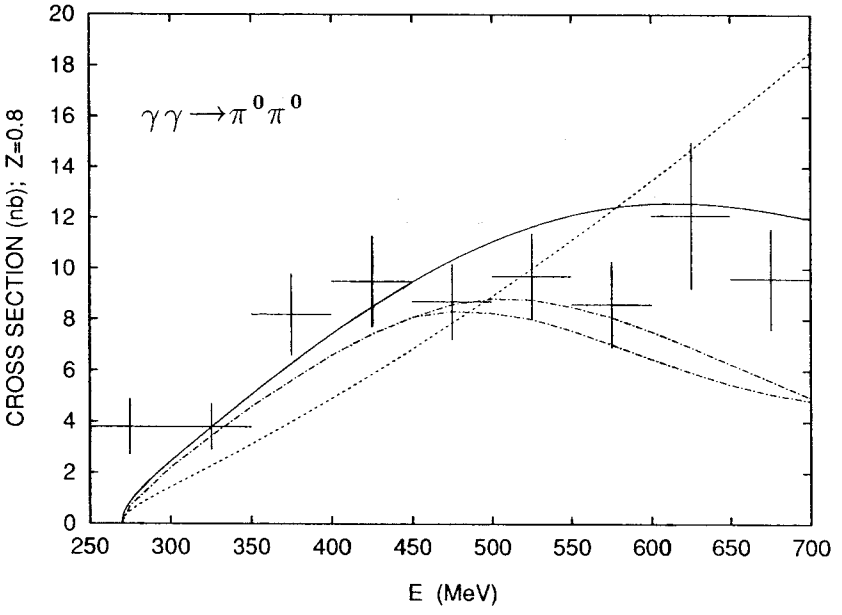

Fig. 5. The $\gamma\gamma \to \pi^0\pi^0$ cross section $\sigma(|\cos\theta| \leqslant Z)$ as a function of the center-of-mass energy E at $Z = 0.8$, together with the data from the Crystal Ball experiment [9]. The errors shown are statistical only. The solid line is the full two-loop result, and the dashed line results from the one-loop calculation [1,2]. The band denoted by the dash-dotted lines is the result of the dispersive calculation by Pennington (Fig. 23 in Ref. [12]).

The integrals $\Delta_{A,B}(s,t,u)$ contain contributions from the two-loop box and acnode diagrams displayed in Fig. 4. It turns out that these contributions are very small for the cross sections below $\sqrt{s} \leqslant 400$ MeV, both for $\gamma\gamma \to \pi^0\pi^0$ (0.1% at 400 MeV) and for the crossed channel $\gamma\pi^0 \to \gamma\pi^0$ (1.5% at 400 MeV). Therefore, one obtains a rather compact and accurate representation of the two-loop amplitudes by simply setting $\Delta_{A,B} = 0$ in $U_{A,B}$ [5].

7.2. *The cross section* $\gamma\gamma \to \pi^0\pi^0$

In Fig. 5 we display the data for the cross section $\sigma(s; |\cos\theta| \leqslant Z = 0.8)$ as determined in the Crystal Ball experiment [9]. They are shown as a function of the center-of-mass energy $E = \sqrt{s}$. The solid line denotes the two-loop result, evaluated[6] with the amplitudes (7.2)–(7.9). For the low-energy constants a_1^r, a_2^r and b^r we have used the values from column 6 in Table 2, and the values of $\bar{l}_i$ are the ones displayed in Table 1. Shown is furthermore, with a dashed line, the one-loop result [1], obtained by setting $U_{A,B} = P_{A,B} = 0$, see also Appendix B. Finally, the dash-dotted lines display the result of a dispersive analysis (Fig. 23 in Ref. [12]). In that calculation, use was made of the $I = 0, 2$ S-wave $\pi\pi$ phase shifts from Ref. [32] (these phase shifts satisfy constraints imposed by Roy-type equations [33]).

[5] An analogous result holds for the elastic $\pi\pi$ scattering amplitude, which contains unitarity contributions with t- and u-channel cuts which are negligible below $E \simeq 500$ MeV for S-waves.

[6] We use $F_\pi = 93.2$ MeV, $M_\pi = M_{\pi^0} = 135$ MeV, unless stated otherwise.

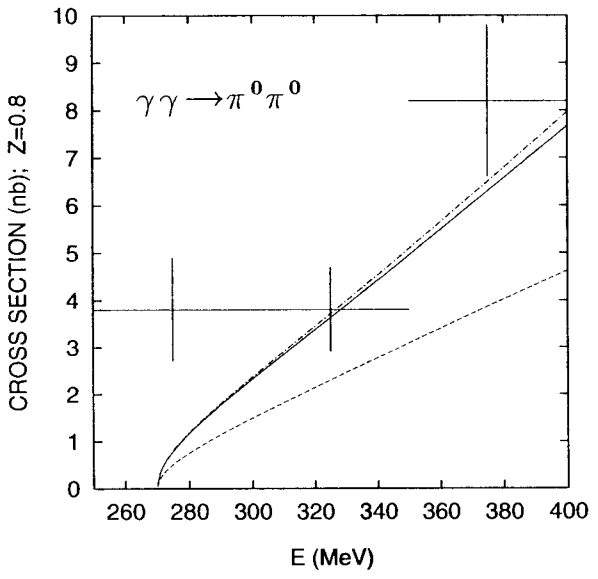

Fig. 6. The dependence of the $\gamma\gamma \to \pi^0\pi^0$ cross section $\sigma(|\cos\theta| \leqslant Z)$ on the constants $\bar{l}_i$, at $Z = 0.8$. The solid line denotes the two-loop result with the standard values for $\bar{l}_i$ displayed in Table 1 (without contributions from resonance exchange, and with $\Delta_{A,B} = 0$), whereas the dashed line is evaluated at $\bar{l}_i = 0$. The dash-dotted line has $\bar{l}_{1,3} = 0$ and the other $\bar{l}_i$ at their standard values.

The two-loop result thus agrees well with the data and with the dispersive analysis of Pennington [12] in the low-energy region.

We found it interesting to see which contributions are responsible for the increase in amplitude and cross section near the threshold. In Fig. 6, we display with a solid line the cross section, evaluated at $\Delta_{A,B} = 0$ and without resonance exchange. [The change compared to the full result (solid line in Fig. 5) is 0.2 nb at $E = 400$ MeV and thus negligible.] The dashed line corresponds to $\bar{l}_i = 0$, and the dash-dotted line is obtained by setting $\bar{l}_1 = \bar{l}_3 = 0$. We conclude that the increase is due to $\bar{l}_2$, $\bar{l}_4$ and $\bar{l}_\Delta = \bar{l}_6 - \bar{l}_5$. To make this statement more quantitative, we note that the dependence of the cross section on the $\bar{l}_i$-values can been summarized with the expression

$$\begin{aligned}
\sigma^{2\text{loops}}(s) &\simeq N\sigma^{1\text{loop}}(s)\,, \\
N &= 1 + (-5.8 + 5.0\bar{l}_1 + 4.9\bar{l}_2 - 0.2\bar{l}_3 + 5.4\bar{l}_4 + 3.7\bar{l}_\Delta) \times 10^{-2} \\
&= 1 - 0.058 - 0.040 + 0.283 - 0.005 + 0.232 + 0.100 \\
&\simeq 1.51\,, \qquad (7.10)
\end{aligned}$$

which is accurate to a few percent up to 450 MeV. The analogous expression for the helicity amplitude H_{++} at the physical threshold $s = 4M_\pi^2$ reads

$$\begin{aligned}
H_{++}^{2\text{loops}} &= NH_{++}^{1\text{loop}}\,, \\
N &= 1 + (2.5 + 0.6\bar{l}_1 + 1.2\bar{l}_2 - 0.2\bar{l}_3 + 2.7\bar{l}_4 + 2.7\bar{l}_\Delta) \times 10^{-2} \\
&= 1 + 0.025 - 0.005 + 0.068 - 0.006 + 0.114 + 0.073 \\
&\simeq 1.27\,, \qquad (7.11)
\end{aligned}$$

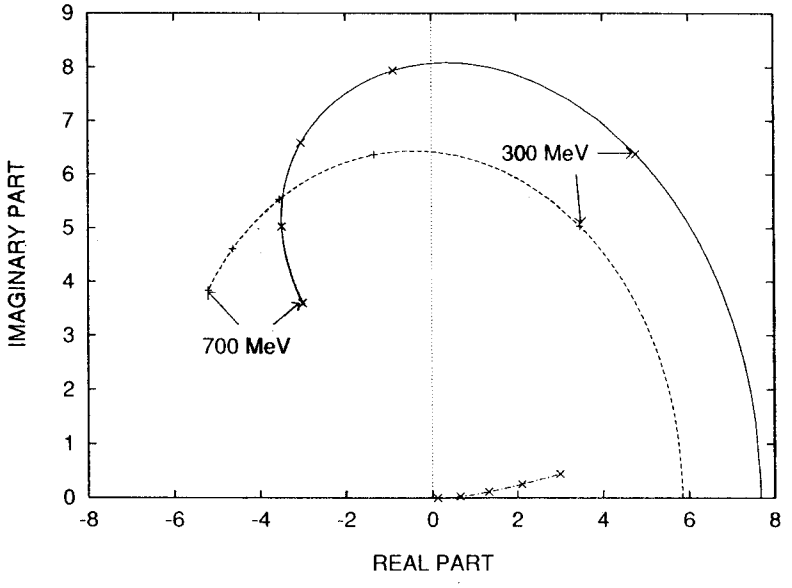

Fig. 7. Real and imaginary part of the amplitudes $\pm 10^2 M_\pi^2 H_{+\pm}$ at $t = u$. The solid line is for $10^2 M_\pi^2 H_{++}$. It incorporates all contributions except $\Delta_{A,B}$. The dashed line is the same amplitude for the one-loop case, and the dash-dotted line is for $-10^2 M_\pi^2 H_{+-}$ with the same input as the solid line. Finally, the crosses refer to the center-of-mass energy of the $\pi^0\pi^0$ system in 100 MeV steps.

with

$$M_\pi^2 H_{++}^{1\text{loop}} = 5.8 \times 10^{-2}. \tag{7.12}$$

The contributions from $\bar{l}_1, \bar{l}_2$ are $\pi\pi$ rescattering effects. They amount to a 24% increase in the cross section (out of 51%) and to 6% in H_{++} (out of 27%). The renormalization of F_π (contribution from $\bar{l}_4$) amounts to a 23% increase in σ.

7.3. *The amplitudes: numerical results*

To get more insight into the characteristics of the two-loop corrections, we display in Fig. 7 the real and imaginary part of the helicity amplitudes $\pm 10^2 M_\pi^2 H_{+\pm}$ at $t = u$. The solid line shows $10^2 M_\pi^2 H_{++}$. It incorporates all contributions except $\Delta_{A,B}$. The dashed line is the same amplitude for the one-loop case, and the dash-dotted line is for $-10^2 M_\pi^2 H_{+-}$ with the same input as for the solid line. The curves start at $E = 2M_\pi$, and the crosses refer to the center-of-mass energy of the $\pi^0\pi^0$ system in 100 MeV steps. The amplitude H_{++} changes very rapidly just above threshold and is nearly purely imaginary in the region 350 MeV $\leqslant E \leqslant$ 400 MeV. As expected, the amplitude H_{+-} which starts out with a D-wave term is very small at low energies. Resonance exchange adds to H_{++} a positive real part, thus increasing the cross section below $\sim$ 400 MeV and decreasing it above this energy.

In Fig. 8, we display the quantity $10^2 M_\pi^2 H_{++}$ at $t = u$ as a function of s/M_π^2. Above the threshold $s = 4M_\pi^2$, the modulus is shown. The solid (dashed) line denotes the full two-loop (one-loop) result. While the two-loop contribution to the modulus is below 30% in the threshold region, it modifies H_{++} substantially (percentage-wise) at $s = 0$,

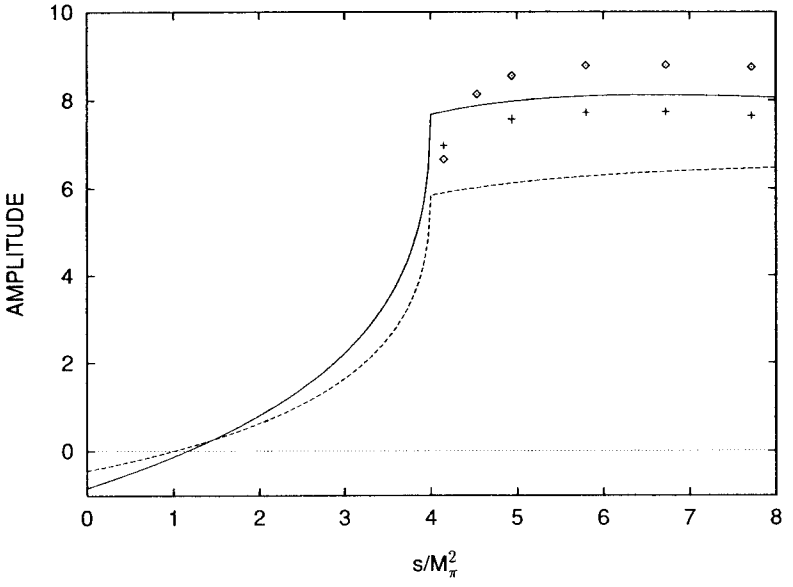

Fig. 8. The $\gamma\gamma \to \pi^0\pi^0$ amplitude as a function of s/M_π^2 at $t = u$. For $s \leqslant 4M_\pi^2$ the quantity shown is $10^2 M_\pi^2 H_{++}$ and for $s \geqslant 4M_\pi^2$ we display $10^2 M_\pi^2 |H_{++}|$. The solid line is the result of the two-loop calculation and the dashed line is the one-loop result. The symbols ($\diamond$, +) refer to the work of Pennington [12]: $\diamond$ (+) is from Fig. 19 (23) in that article.

where the amplitude is small, see also the discussion below. Furthermore, we note that the zero at $s = M_\pi^2$, which occurs in the one-loop approximation Eq. (B.6), is only slightly modified by the loop corrections. Finally, we display with $\diamond$ (+) the modulus of the S-wave projected part of H_{++}, taken from Fig. 19 (23) in Ref. [12].

7.4. *Error estimates and range of validity of the chiral representation*

The uncertainty in the amplitude has two sources. Firstly, the low-energy constants $\bar{l}_i$, $h_\pm^r$ and h_s^r used above contain certain errors. For the $\bar{l}_i$, these are displayed in Table 1. The systematic errors in the low-energy couplings at order E^6 have been estimated in the previous section, see Eq. (6.6). Secondly, we are concerned here with an expansion in powers of the quark masses and of the external momenta. Higher-order terms in this expansion (three loops and beyond) will change the cross section accordingly.

We discuss first the effect of the uncertainty in the low-energy constants and concentrate for simplicity on $h_\pm^r$ and h_s^r. In Fig. 9 we show the variation of the cross section according to the error estimates in Eq. (6.6). The calculation is done at $\Delta_{A,B} = 0$. The dashed lines embrace the region generated by assigning all possible combinations of signs to the systematic errors in the couplings $h_\pm^r$ and h_s^r according to Eq. (6.6). The dash-dotted line corresponds to the central value in (6.6).

It is clearly seen that, below 400 MeV, the uncertainties in $h_\pm^r$ and in h_s^r do not matter. (Since we estimate the couplings with resonance saturation, this is a reformulation of earlier findings [34–39].) Varying the scale at which resonance saturation is assumed between 500 MeV and 1 GeV results also in a negligible change in the cross section below $E = 400$ MeV. Beyond this energy, the uncertainty becomes more pronounced.

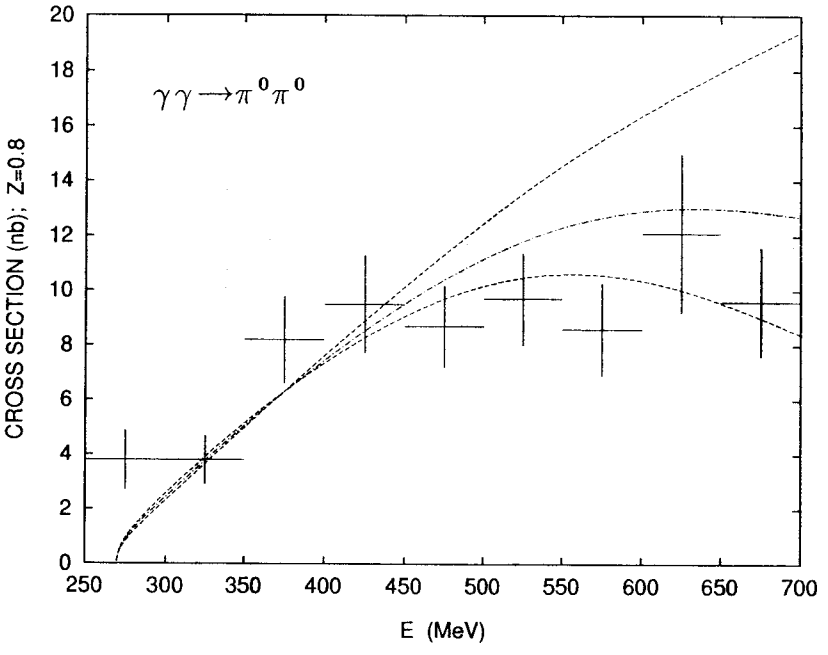

Fig. 9. The uncertainty in the value of the $\gamma\gamma \to \pi^0\pi^0$ cross section $\sigma(|\cos\theta| \leqslant Z)$ at $Z = 0.8$, evaluated from the two-loop amplitude at $\Delta_{A,B} = 0$. The data are from the Crystal Ball experiment [9]. The dashed lines embrace the region generated by assigning all possible combinations of signs to the systematic errors in the couplings $h^r_\pm$ and h^r_s according to Eq. (6.6). The dash-dotted line corresponds to the central values in (6.6). Above $E \simeq 400$ MeV, the major part of the uncertainty in the cross section is generated by the error in h^r_s.

Because the contribution from H_{+-} is tiny (see Fig. 7), only h^r_+ and h^r_s really count. One might thus be tempted to extract these couplings from more accurate data in the range E = (400–600) MeV. This would be interesting, because h^r_+ determines the difference of the electric and magnetic polarizabilities of the neutral pion at two-loop order, see below. However, in this energy range where $s \simeq (9\text{–}20)M_\pi^2$, h^r_s is much more important than h^r_+. It will, therefore, be rather difficult to extract h^r_+ reliably in this manner [13]. On the other hand, it would be interesting to perform a combined analysis of the two related processes $\gamma\gamma \to \pi^0\pi^0$ and $\eta \to \pi^0\gamma\gamma$ [25] in the framework of $SU(3)_L \times SU(3)_R$ in order to obtain maximal information on the low-energy coupling constants which enter these amplitudes[7].

Turning now to the corrections from yet higher orders, we use the fact that $\sigma^{2\text{loops}}/\sigma^{1\text{loop}} \simeq (1+\epsilon)^2$ with $\epsilon \simeq 0.25$ and estimate $\sigma/\sigma^{1\text{loop}} \simeq (1-\epsilon)^{-2}$. This amounts to a 15–20% uncertainty in the two-loop result below 400 MeV. At higher energies, the error in the cross section is more difficult to assess. It may well turn out, however, that a more precise determination of the low-energy couplings leads to the conclusion that the chiral representation of the amplitude at the two-loop level is even valid up to E = (600–700) MeV in this channel.

[7] We thank J. Bijnens, M. Knecht and J. Stern for pointing this out to us.

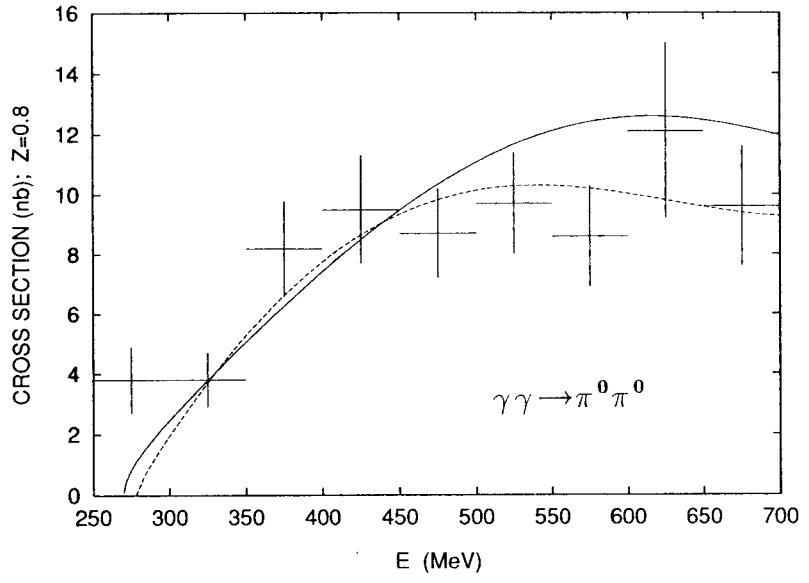

Fig. 10. The Compton cross section $\gamma\pi^0 \to \gamma\pi^0$ as a function of the center-of-mass energy $E_{\gamma\pi}$. The solid line is the result of the two-loop calculation and the dashed line is the one-loop result. The dash-dotted line refers to the two-loop calculation at $h^r_\pm = h^r_s = 0$, and the dotted line has $H_{+-} = 0$ in a full two-loop calculation.

8. Compton scattering and pion polarizabilities

The amplitudes A and B are analytic functions of s and t. At $s \leqslant 0$, they describe Compton scattering (see Fig. 1),

$$\gamma(q_1)\pi^0(p_1) \to \gamma(q_2)\pi^0(p_2)\,. \tag{8.1}$$

We discuss this reaction in the present section, where we also work out the (neutral) pion polarizabilities at next-to-leading order.

8.1. Compton scattering

The cross section $\gamma\gamma \to \pi^0\pi^0$ receives a substantial correction near threshold due to $\pi\pi$ final-state interactions – which are absent in Compton scattering. Are then the two-loop contributions small in this channel? Fig. 8 shows that this is not the case: in the one-loop approximation, the amplitude H_{++} is one order of magnitude larger in the $\gamma\gamma \to \pi^0\pi^0$ channel than at Compton threshold. Therefore, even tiny corrections in $\gamma\gamma \to \pi^0\pi^0$ may appear large in Compton scattering [39]. In Fig. 10 we display the cross section $\sigma^{\gamma\pi^0\to\gamma\pi^0}$ as a function of the center-of-mass energy $E_{\gamma\pi}$. The solid line shows the result of the two-loop calculation and the dashed line displays the one-loop approximation. They differ by one order of magnitude already near threshold. This is mainly due to the effect of the low-energy constant h^r_- in H_{+-} (omega-exchange in the language of resonance saturation [39]). Putting H_{+-} to zero results in $\sigma^{\gamma\pi^0\to\gamma\pi^0} = 0.7$ nb at $E_{\gamma\pi} = 350$ MeV (dotted line). Purely two-loop effects however also change

the cross section by roughly a factor of two at $E_{\gamma\pi} = 350$ MeV (dash-dotted line, evaluated at $h^r_\pm = h^r_s = 0$).

In summary, the Compton amplitude is tiny at leading order, and it is therefore rather unstable against the corrections generated by higher-order terms.

8.2. *Pion polarizabilities*

For a composite system it is customary to include the electric and magnetic polarizabilities among the fundamental parameters – such as the electric charge, the magnetic moment and the mass – characterizing the low-energy limit of the coupling with the photon in the Compton amplitude. Hadrons are no exception, hence the theoretical description of their dynamics can be tested through the experimental determination of the hadron polarizabilities [40]. To set notation, we first consider Compton scattering for charged pions,

$$\gamma(q_1)\pi^+(p_1) \to \gamma(q_2)\pi^+(p_2)\,, \tag{8.2}$$

in the laboratory system $p_1^0 = M_\pi$. (In order to simplify the notation, we use the symbol M_π to denote both the charged and the neutral pion mass.) The electric ($\bar\alpha_\pi$) and magnetic ($\bar\beta_\pi$) polarizabilities are obtained by expanding the Compton amplitude at threshold,

$$f^C = 2\left[\boldsymbol{\epsilon}_1\cdot\boldsymbol{\epsilon}_2^\star\left(\frac{\alpha}{M_\pi} - \bar\alpha_\pi\omega_1\omega_2\right) - \bar\beta_\pi\left(\boldsymbol{q}_1\times\boldsymbol{\epsilon}_1\right)\cdot\left(\boldsymbol{q}_2\times\boldsymbol{\epsilon}_2^\star\right) + \ldots\right] \tag{8.3}$$

with $q_i^\mu = (\omega_i, \boldsymbol{q}_i)$. In terms of the helicity components (B.4), one has

$$\bar\alpha_\pi \pm \bar\beta_\pi = -\frac{\alpha}{M_\pi}\bar H^C_{+\mp}(s=0, t=M_\pi^2)\,, \tag{8.4}$$

where the bar denotes the amplitude with the Born term removed[8]. For neutral pions, one uses the analogous definition,

$$\bar\alpha_{\pi^0} \pm \bar\beta_{\pi^0} = \frac{\alpha}{M_\pi} H_{+\mp}(0, M_\pi^2)\,, \tag{8.5}$$

or, in terms of A and B,

$$\begin{aligned}
\bar\alpha_{\pi^0} &= \frac{\alpha}{2M_\pi}\left(A + 16M_\pi^2 B\right)\Big|_{s=0,t=M_\pi^2}\,,\\
\bar\beta_{\pi^0} &= -\frac{\alpha}{2M_\pi}A\Big|_{s=0,t=M_\pi^2}\,.
\end{aligned} \tag{8.6}$$

Below we also use the notation

$$\begin{aligned}
(\alpha\pm\beta)^C &= \bar\alpha_\pi \pm \bar\beta_\pi\,,\\
(\alpha\pm\beta)^N &= \bar\alpha_{\pi^0} \pm \bar\beta_{\pi^0}\,.
\end{aligned} \tag{8.7}$$

[8] In $\bar H^C_{+-}$ first set $t = M_\pi^2$, then $s \to 0$. We use the Condon–Shortley phase convention.

An unsubtracted forward dispersion relation for the amplitude B gives with (2.11)

$$(\alpha+\beta)^N = \frac{M_\pi}{\pi^2}\int_{4M_\pi^2}^{\infty}\frac{ds'}{(s'-M_\pi^2)^2}\sigma_{\rm tot}^{\gamma\pi^0}(s')\,, \tag{8.8}$$

and analogously for the charged channel.

8.3. Data on pion polarizabilities

There exist up to now two determinations of charged pion polarizabilities via measurement of the Compton amplitude. At Serpukhov [41], radiative pion–nucleus scattering $\pi^- A \to \pi^-\gamma A$ has been used. Here the incident pion scatters from a virtual photon in the Coulomb field of the nucleus. In the pion production process $\gamma p \to \gamma\pi^+ n$ examined at the Lebedev Institute [42], the incoming photon scatters from a virtual pion. Analyzing the data with the constraint $(\alpha+\beta)^C = 0$ gives[9]

$$(\alpha-\beta)^C = \begin{cases} 13.6 \pm 2.8 & [41]\,, \\ 40 \pm 24 & [42]\,. \end{cases} \tag{8.9}$$

The Serpukhov data have been analyzed also relaxing the constraint $(\alpha+\beta)^C = 0$, with the result

$$\begin{aligned} (\alpha+\beta)^C &= \ 1.4 \pm 3.1(\text{stat.}) \pm 2.5(\text{sys.}) \ \ [43]\,, \\ (\alpha-\beta)^C &= 15.6 \pm 6.4(\text{stat.}) \pm 4.4(\text{sys.}) \ \ [43]\,. \end{aligned} \tag{8.10}$$

Here we have converted the value quoted for $\bar\beta_\pi$ into a number for $(\alpha-\beta)^C$, adding the errors in quadrature.

Furthermore, also the process $\gamma\gamma \to \pi\pi$ may be used to obtain information on the polarizabilities. Since in this case the amplitude at low energies is mainly sensitive to S-wave scattering, only $(\alpha-\beta)^{C,N}$ can be determined from the presently available [8,9] data. In Ref. [16], unitarized S-wave amplitudes have beeen constructed, which contain $(\alpha-\beta)^{C,N}$ as adjustable parameters. A simultaneous fit to Mark II and Crystal Ball data gives

$$\begin{aligned} (\alpha-\beta)^C &= \ 4.8 \pm 1.0 \ \ [16]\,, \\ (\alpha-\beta)^N &= -1.1 \pm 1.7 \ \ [16]\,, \end{aligned} \tag{8.11}$$

where we have taken into account that the definition of the polarizabilities in Ref. [16] is 4π larger than the one used here, see Ref. [44], Eq. (1).

The value (8.11) for $(\alpha-\beta)^C$ is consistent with Refs. [42,43] within $1\frac{1}{2}$ standard deviations, but not consistent with Ref. [41]. The large relative error in $(\alpha-\beta)^N$ reflects the fact that the threshold amplitude $\gamma\gamma \to \pi^0\pi^0$ is quite insensitive to large relative changes at the Compton threshold, as we discussed above (see also Fig. 10

[9] We express the polarizabilities in units of 10^{-4} fm^3 throughout.

in Ref. [13]). The determination of $(\alpha-\beta)^{C,N}$ from $\gamma\gamma \to \pi\pi$ furthermore suffers from uncertainties which we find difficult to estimate in the approach used by Kaloshin and Serebryakov [16], which does not provide a systematic way to control the inherent uncertainties in the model amplitude used to fit the data. It might be interesting to merge dispersion relations and CHPT at next-to-leading order in the chiral expansion. This method [45,13], which does provide a control on the approximations made, would then allow for an experimental determination of $(\alpha-\beta)^{C,N}$ at order E, requiring, however, a two-loop evaluation of $\gamma\gamma \to \pi^+\pi^-$.

In Ref. [46], the bound $|\bar{\alpha}_{\pi^0}| < 35$ has been obtained from a study of the $e^+e^- \to \pi^0\pi^0\gamma$ reaction.

Finally, information on the charged pion polarizabilities may be obtained from $\gamma\gamma \to \pi^+\pi^-$ data in the following manner [47]. Both the one-loop expression for the transition amplitude and the leading-order expression for $\bar{\alpha}_\pi$ and $\bar{\beta}_\pi$ contain the low-energy constant $\bar{l}_\triangle$ as the only free parameter. Extracting it from a fit to the cross section then determines $\bar{\alpha}_\pi$ and $\bar{\beta}_\pi$ at this order. The result [47] $\bar{l}_\triangle = 2.3 \pm 1.7$ agrees within the error with the value $\bar{l}_\triangle = 2.7$ used in the present work – the corresponding numerical values for the leading-order expressions of $(\alpha \pm \beta)^C$ therefore also agree. The cross section in the threshold region is dominated by the Born term contribution and is, therefore, rather insensitive to $\bar{l}_\triangle$ [1]. This is the main reason for the large uncertainty in this determination of $\bar{l}_\triangle$.

8.4. *Chiral expansion of pion polarizabilities*

The one-loop result is

$$
\begin{aligned}
(\alpha+\beta)^C &= 0\,,\\
(\alpha+\beta)^N &= 0\,,\\
(\alpha-\beta)^C &= \frac{\alpha \bar{l}_\triangle}{24\pi^2 M_\pi F^2} = 5.3\,,\\
(\alpha-\beta)^N &= -\frac{\alpha}{48\pi^2 M_\pi F^2} = -1.0\,.
\end{aligned}
\tag{8.12}
$$

Here we have identified F with the physical value of the pion decay constant, and we have used the charged pion mass to evaluate of $(\alpha-\beta)^C$. It is straightforward to determine from the amplitudes given in the previous section the neutral pion polarizabilities to two loops. We find

$$
(\alpha \pm \beta)^N = \frac{\alpha}{16\pi^2 M_\pi F_\pi^2}\left\{c_\pm + \frac{M_\pi^2 d_\pm}{16\pi^2 F_\pi^2} + O(M_\pi^4)\right\}\,,
\tag{8.13}
$$

with

$$
\begin{aligned}
c_+ &= 0\,,\\
c_- &= -\tfrac{1}{3}\,,
\end{aligned}
$$

Table 3
Neutral pion polarizabilities to two loops in units of 10^{-4} fm^3. The contribution due to chiral logarithms, listed in the fifth column with bracketed numbers, is included in the two-loop result quoted in column four.

	$O(E^{-1})$	$O(E)$				
	1 loop	$h^r_\pm$	2 loops	chiral logs	Total	Uncertainty
$(\alpha+\beta)^N$	0.00	1.00	0.17	[0.21]	$\simeq$ 1.15	±0.30
$(\alpha-\beta)^N$	−1.01	−0.58	−0.31	[−0.18]	$\simeq$ −1.90	±0.20
$\bar{\alpha}_{\pi^0}$	−0.50	0.21	−0.07	[0.01]	$\simeq$ −0.35	±0.10
$\bar{\beta}_{\pi^0}$	0.50	0.79	0.24	[0.20]	$\simeq$ 1.50	±0.20

$$d_+ = 8h^r_- - \tfrac{1}{648}\{144l[l+2\bar{l}_2] + 96l + 288\bar{l}_2 + 113 + \Delta_+\}\,,$$
$$d_- = h^r_+ + \tfrac{1}{648}\{144l(3\bar{l}_\Delta - 1) + 36[8\bar{l}_1 - 3\bar{l}_3 - 12\bar{l}_4 + 12\bar{l}_\Delta] + 43 + \Delta_-\}\,. \tag{8.14}$$

The quantities $\Delta_\pm$ (generated by the contributions from $\Delta_{A,B}$ in (7.3, 7.8)) are pure numbers, independent of l and of $\bar{l}_i$. The numerical results are displayed in Table 3. The second column contains the contribution at order E^{-1}, and the third to fifth columns display the terms of order E. The total values are given in column 6. (The two-loop contribution $(\alpha+\beta)^N = 0.18$ reported earlier [48] and quoted in Ref. [39] corresponds to slightly different values of $\bar{l}_1$ and $\bar{l}_2$.) Finally, our estimate of the errors is shown in the last column. These are obtained in the same manner as the ones for the couplings $h^r_\pm$ and h^r_s in Eq. (6.6). We have not considered correlations in these uncertainties, which do also not contain effects from higher orders in the quark mass expansion.

The contribution from the chiral logarithms present in the low-energy expansion of the polarizabilities deserves a comment. As we discussed earlier, the $\ln^2 M_\pi^2/\mu^2$ terms occur in a particular combination which is dictated by the general structure of the renormalized amplitude,

$$(\alpha \pm \beta)^N_{2\text{loops}} = C_\pm L_\chi + \ldots\,,$$
$$L_\chi = \frac{\alpha M_\pi}{(16\pi^2 F_\pi^2)^2} \ln M_\pi^2/\mu^2 \{\ln M_\pi^2/\mu^2 + 2\bar{l}_2\}\,.$$

Here the ellipsis denotes further single logarithms and terms of order M_π, and $C_\pm$ are Clebsch-Gordan coefficients. These terms are potentially very large,

$$L_\chi = -1.14 \times 10^{-4}\ \text{fm}^3$$

at $\mu = M_\rho$. It turns out that C_+ is small, whereas C_- even vanishes, see (8.13), (8.14). We have listed the sum of the $\ln^2 M_\pi^2/\mu^2$ and $\ln M_\pi^2/\mu^2$ terms at the scale $\mu = M_\rho$ in the fifth column of Table 3–these contributions are included in the two-loop result quoted in column four.

The low-energy constants determined in Ref. [35] give for the contributions from $h^r_\pm$

$$(\bar{\alpha}_{\pi^0}, \bar{\beta}_{\pi^0}) = \begin{cases} (0.0, 0.72) \text{ vector-mesons (nonet)}, \\ (0.0, 0.50) \text{ chiral quark model}. \end{cases} \tag{8.15}$$

The corresponding entries in column 3 of Table 3 are slightly different than the ones from vector-exchange in Eq. (8.15), because we do not use the nonet-assumption here and include in addition axial-vector exchange. The slight discrepancy with the chiral quark model prediction is not serious, because the systematic uncertainties in that framework are very difficult to assess.

Turning now to a comparison with the data, we note that the two-loop result for $(\alpha-\beta)^N$ agrees within the error bars with the value found by Kaloshin and Serebryakov [16]. As for the charged pion case, the complete expression at order E is not yet available. The chiral logarithms which occur at this order in the low-energy expansion can in principle contribute substantially also here. Therefore, to compare the chiral prediction with the data, a full two-loop calculation is required [49].

9. Comparison with dispersion relations

In this section we compare in some detail the chiral expansion with the dispersive calculation carried out by Donoghue and Holstein [13].
Consider the S-wave amplitude

$$F(s) = \frac{1}{4\pi} \int \mathrm{d}\Omega\, H_{++}(s,t)\,. \tag{9.1}$$

We find from the two-loop representation given above

$$\begin{aligned} F^{\mathrm{CHPT}} &= \frac{2}{sF_\pi^4}\bar{G}_\pi(s)\left\{2F_\pi^2(s-M_\pi^2) + (s^2-M_\pi^4)\bar{J}(s) + C(s,\bar{l}_i)\right\} \\ &\quad + \frac{\bar{l}_\Delta}{24\pi^2F_\pi^4}(s-M_\pi^2)\left(\bar{J}(s) - \frac{1+l}{16\pi^2}\right) + P_F + \Delta_F\,, \\ P_F &= \frac{1}{(16\pi^2F_\pi^2)^2}\left[f_1M_\pi^2 + f_2 s\right], \\ f_1 &= h_+^r - \tfrac{1}{9}\left\{2l + \tfrac{8}{3}\bar{l}_2 - \tfrac{47}{72}\right\}, \\ f_2 &= h_s^r + \tfrac{1}{18}\left\{\tfrac{4}{3}\bar{l}_2 - \tfrac{19}{9}\right\}, \\ l &= \ln\frac{M^2}{\mu^2}\,, \end{aligned} \tag{9.2}$$

where $C(s,\bar{l}_i)$ is displayed in Eq. (7.4), and where Δ_F is the S-wave contribution from $\Delta_{A,B}$. In the region $2M_\pi \leqslant E \leqslant 400$ MeV, the polynomial P_F contributes very little to the amplitude. For the comparison with the dispersive approach in this region we therefore drop it, together with Δ_F.

In the simplest version of their analysis, Donoghue and Holstein write

$$F^{\mathrm{DISP}} = \frac{4\bar{G}_\pi(s)}{3sF_\pi^2}\left\{(2s - M_\pi^2)D_0^{-1}(s) + (s - 2M_\pi^2)D_2^{-1}(s)\right\}$$
$$+ \frac{\bar{l}_\Delta}{36\pi^2 F_\pi^2}\left\{D_0^{-1}(s) - D_2^{-1}(s)\right\}, \tag{9.3}$$

where D_I^{-1} is the Omnès function

$$D_I^{-1} = \frac{1}{1 - k_I s - t_I^{\mathrm{CA}} 16\pi \bar{J}(s)}, \tag{9.4}$$

with

$$k_0 = \frac{1}{25M_\pi^2}, \qquad k_2 = -\frac{1}{30M_\pi^2},$$
$$t_0^{\mathrm{CA}} = \frac{2s - M_\pi^2}{32\pi F_\pi^2}, \qquad t_2^{\mathrm{CA}} = -\frac{s - 2M_\pi^2}{32\pi F_\pi^2}. \tag{9.5}$$

Expanding D_I^{-1} and keeping terms of the same order as in F^{CHPT}, we find (we count k_I as order E^0)

$$F^{\mathrm{DISP}} = \frac{2}{sF_\pi^4}\bar{G}_\pi(s)\left\{2F_\pi^2(s - M_\pi^2) + (s^2 - M_\pi^4)\bar{J}(s) + C^{\mathrm{DISP}}\right\}$$
$$+ \frac{\bar{l}_\Delta}{24\pi^2 F_\pi^4}\left\{(s - M_\pi^2)\bar{J}(s) + \tfrac{2}{3}F_\pi^2 s(k_0 - k_2)\right\} + O(E^4),$$
$$C^{\mathrm{DISP}} = \tfrac{2}{3}F_\pi^2 s[k_0(2s - M_\pi^2) + k_2(s - 2M_\pi^2)]. \tag{9.6}$$

The two representations (9.2) and (9.6) give very similar cross sections up to $E \simeq 400$ MeV. This is at first surprising, because the polynomial $C(s, \bar{l}_i)$ in the chiral representation (9.2) contains rescattering effects which are algebraically quite different from C^{DISP} (e.g., the leading terms $\simeq s^2$ differ by more than a factor of 3). The polynomial multiplying $\bar{l}_\Delta$ is also different in the two representations. The combined effect of these two differences is that the S-wave amplitude (9.6) agrees numerically quite well with (9.2). [Notice that Fig. 3 in Ref. [13] which displays the cross section according to Eq. (9.3) is not correct [51].]

Donoghue and Holstein then refine their representation (9.3) by adding contributions from resonance exchange. Their final result for the cross section agrees very well with our representation below $E = 400$ MeV, see Fig. 11. There we display with a solid line the two-loop result. The dashed line is the result of Donoghue and Holstein (Fig. 2 in Ref. [13]). The two representations differ in the threshold region, because M_π is identified with the charged pion mass by these authors.

There *are* differences in the two representations, though. First, in the dispersive method, higher-order terms are partially summed up. We consider the fact that the cross sections agree as an indication that yet higher orders in the chiral expansion do not affect the amplitude in the threshold region very much. Secondly, CHPT reveals that the amplitude contains chiral logarithms, generated by pion loops. All of these effects

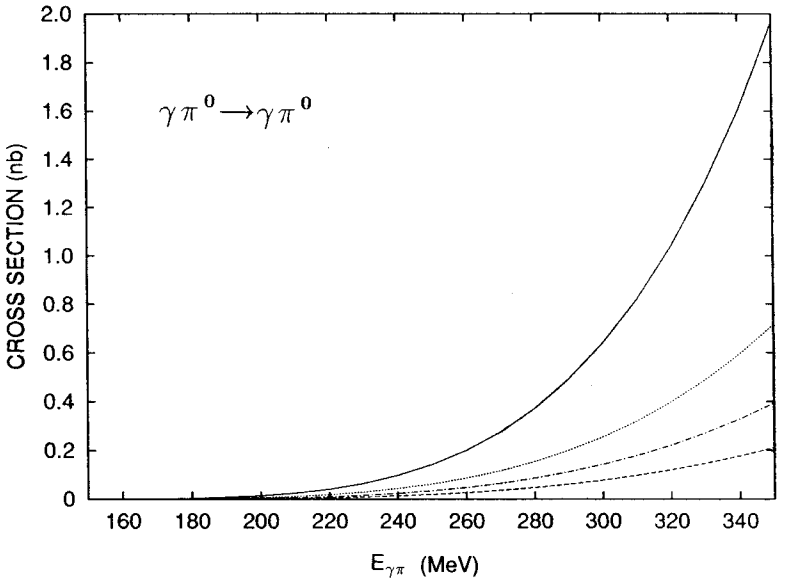

Fig. 11. The $\gamma\gamma \to \pi^0\pi^0$ cross section $\sigma(|\cos\theta| \leqslant Z)$ as a function of the center-of-mass energy at $Z = 0.8$, with the data from the Crystal Ball [9] experiment. The solid line is the two-loop result, whereas the dashed line is taken from the dispersive analysis of Donoghue and Holstein (Fig. 2 in Ref. [13]).

are not incorporated in the dispersive analysis of Ref. [13]. To illustrate, consider the amplitude F at the Compton threshold, where it determines the difference of the electric and magnetic polarizabilities,

$$(\alpha - \beta)^N = \frac{\alpha}{M_\pi} F(0) . \tag{9.7}$$

Numerically, the chiral logarithms amount to a 18% correction to the leading-order term $(\alpha - \beta)^N = -1.01$, see Table 3. The result $(\alpha - \beta)^N = -1.76$ quoted in Ref. [13] corresponds to the one-loop contribution and to vector exchange alone and therefore differs from our value $(\alpha - \beta)^N \simeq -1.90$. In $\bar{\beta}_{\pi^0}$, axial-vectors do not contribute. The logarithms amount to 0.20 in the final result $\bar{\beta}_{\pi^0} \simeq 1.50$ which differs by 20% from the value $\bar{\beta}_{\pi^0} = 1.26$ in Ref. [13].

10. Summary and conclusion

(i) At leading order in the chiral expansion, the amplitude for $\gamma\gamma \to \pi^0\pi^0$ is generated by one-loop graphs [1,2]. In the case of $SU(2)_L \times SU(2)_R \times U(1)$ considered here, it involves the pion decay constant and the pion mass as the only parameters. The corresponding cross section deviates from the data and from dispersive calculations already near threshold.

(ii) The neglected terms in this calculation are related to $\pi\pi$ final-state interactions and to three new low-energy constants $h^r_\pm$ and h^r_s which occur at order E^6 in the effective action.

(iii) To investigate these corrections, we have evaluated the next-to-leading order terms in the chiral expansion (two-loop diagrams) and have estimated the new couplings

in the standard manner [4,30] by resonance saturation ($J^{PC} = 0^{++}$, 1^{--}, 1^{+-}, 2^{++}).

(iv) The improved cross section agrees rather well with the data and with dispersion theoretic calculations at and also substantially above the threshold region, see Fig. 5 and Fig. 11. The enhancement in the cross section is mainly due to $\pi\pi$ rescattering and to the renormalization of the pion decay constant.

(v) The two-loop corrections are not unduly large – their size is similar to the corresponding next-to-leading order correction in the isospin zero $\pi\pi$ scattering amplitude [4] and in the scalar form factor of the pion [21].

(vi) The couplings $h^r_\pm$ and h^r_s contribute with a negligible amount below $E = 400$ MeV [34–39]. Above this energy, the inherent uncertainty in h^r_s becomes more important (Fig. 9). The influence of $h^r_\pm$ is quite small also in the region 400 MeV $\leqslant E \leqslant$ 600 MeV.

(vii) The amplitude for the crossed reaction $\gamma\pi^0 \to \gamma\pi^0$ is small at the threshold $E_{\gamma\pi} = M_\pi$. As a result of this, the one-loop representation is substantially distorted by the next-to-leading order terms, although there are no final-state interactions in this case. The dominant effect is due to h^r_- (omega exchange $\gamma\pi^0 \to \omega \to \gamma\pi^0$ in the language of resonance saturation [39]).

(viii) The quark mass expansion of the pion polarizabilities $\bar{\alpha}_{\pi^0}$ and $\bar{\beta}_{\pi^0}$ contains chiral logarithms $\sim M_\pi \ln^2 M_\pi$ and $\sim M_\pi \ln M_\pi$ which contribute substantially to $\bar{\alpha}_{\pi^0} \pm \bar{\beta}_{\pi^0}$, although their effect is suppressed by small Clebsch-Gordan coefficients. The effect of the low-energy constants $h^r_\pm$ on the value of $\bar{\alpha}_{\pi^0} \mp \bar{\beta}_{\pi^0}$ is large. It will presumably be difficult to extract these couplings from low-energy $\gamma\gamma \to \pi^0\pi^0$ data alone and to determine in this manner the polarizabilities at two-loop order [13].

(ix) The DAFNE facility [17,18] will have the opportunity to test the chiral predictions at next-to-leading order in much more detail than is possible with present data.

Acknowledgement

It is a pleasure to thank for useful discussions with or support from Ll. Ametller, D. Babusci, J. Bijnens, A. Bramon, G. D'Ambrosio, J.F. Donoghue, G. Ecker, M. Egger, H. Genz, O. Hänni, A. Held, F. Jegerlehner, M. Knecht, I. Kušar, H. Leutwyler, L. Maiani, G.J. van Oldenborgh, G. Pancheri, M. Pennington, J. Stern and G. Weiglein. One of the authors (M.E.S.) thanks the Magnus Ehrnrooth Foundation for a grant.

Appendix A. Decomposition of $V^{\mu\nu}$

Here we briefly discuss the correlator

$$V_{\mu\nu} = i \int \mathrm{d}x\, \mathrm{e}^{-i(q_1 x + q_2 y)} \langle \pi^0(p_1)\pi^0(p_2)\mathrm{out} \mid T j_\mu(x) j_\nu(y) \mid 0 \rangle . \tag{A.1}$$

We decompose $V^{\mu\nu}$ into Lorentz and parity invariant amplitudes

$$V_{\mu\nu} = V_0 g_{\mu\nu} + V_1 q_{1\mu} q_{1\nu} + V_2 q_{1\mu} q_{2\nu} + V_3 q_{1\mu} \Delta_\nu + V_4 q_{1\nu} q_{2\mu} + V_5 q_{1\nu} \Delta_\mu + V_6 q_{2\mu} q_{2\nu}$$
$$+ V_7 q_{2\mu} \Delta_\nu + V_8 q_{2\nu} \Delta_\mu + V_9 \Delta_\mu \Delta_\nu ,$$
$$\Delta_\mu = (p_1 - p_2)_\mu$$
$$V_i = V_i(s, \nu) , \qquad i = 0, \ldots, 9 ,$$
$$s = (q_1 + q_2)^2 , \qquad t = (p_1 - q_1)^2 , \qquad u = (p_2 - q_1)^2 ,$$
$$\nu = t - u . \tag{A.2}$$

From Bose symmetry

$$V_{\mu\nu}(\Delta, q_1, q_2) = V_{\mu\nu}(-\Delta, q_1, q_2) = V_{\nu\mu}(\Delta, q_2, q_1) \tag{A.3}$$

we find

$$V_i(s, \nu) = V_i(s, -\nu) , \qquad i = 0, 1, 2, 4, 6, 9 ,$$
$$V_i(s, \nu) = -V_i(s, -\nu) , \qquad i = 3, 5, 7, 8 , \tag{A.4}$$

and

$$V_6 = V_1 , \qquad V_5 = -V_7 , \qquad V_8 = -V_3 . \tag{A.5}$$

The Ward identity

$$q_1^\mu V_{\mu\nu} = 0 \tag{A.6}$$

gives with $q_i^2 = 0$

$$2V_0 + sV_4 - \nu V_5 = 0 ,$$
$$sV_1 + \nu V_3 = 0 ,$$
$$sV_7 - \nu V_9 = 0 . \tag{A.7}$$

The second Ward identity $q_2^\nu V_{\mu\nu} = 0$ is then automatically satisfied by Bose symmetry. We are left with four independent form factors which we take to be

$$A = -V_4 , \qquad B = V_9/2s , \qquad C = V_2 , \qquad D = V_3/s . \tag{A.8}$$

Insertion into (A.2) gives the decomposition Eq. (2.4) in the text.

Appendix B. $\gamma\gamma \to \pi\pi$ to one loop

For convenience, we collect here the one-loop expressions for the amplitudes $\gamma\gamma \to \pi^0\pi^0, \pi^+\pi^-$ [1,2].

B.1. $\gamma\gamma \to \pi^+\pi^-$

The matrix element for

$$\gamma(q_1)\gamma(q_2) \to \pi^+(p_1)\pi^-(p_2) \tag{B.1}$$

is given by

$$\langle \pi^+(p_1)\pi^-(p_2)\text{out} \mid \gamma(q_1)\gamma(q_2)\text{in}\rangle = i(2\pi)^4\delta^4(P_f - P_i)T^C, \tag{B.2}$$

with

$$\begin{aligned} T^C &= e^2\epsilon_1^\mu\epsilon_2^\nu V^C_{\mu\nu}\,, \\ V^C_{\mu\nu} &= i\int \mathrm{d}x\, \mathrm{e}^{-i(q_1x+q_2y)}\langle \pi^+\pi^-\text{out} \mid Tj_\mu(x)j_\nu(y) \mid 0\rangle \\ &= A^C T_{1\mu\nu} + B^C T_{2\mu\nu} + C^C T_{3\mu\nu} + D^C T_{4\mu\nu}\,. \end{aligned} \tag{B.3}$$

The tensors $T_{i\mu\nu}$ are defined in (2.4). The helicity amplitudes are

$$\begin{aligned} H^C_{++} &= A^C + 2(4M_\pi^2 - s)B^C\,, \\ H^C_{+-} &= \frac{8(M_\pi^4 - tu)}{s}\,B^C\,. \end{aligned} \tag{B.4}$$

The low-energy expansion of the amplitudes A^C, B^C reads [1] in $SU(2)_L \times SU(2)_R \times U(1)$ with the Condon–Shortley phase convention

$$\begin{aligned} A^C &= -\left\{\frac{1}{M_\pi^2 - t} + \frac{1}{M_\pi^2 - u}\right\} - \frac{2}{F^2}\left\{\bar{G}(s) + \frac{\bar{l}_\Delta}{48\pi^2}\right\} + O(E^2)\,, \\ B^C &= -\frac{1}{2s}\left\{\frac{1}{M_\pi^2 - t} + \frac{1}{M_\pi^2 - u}\right\} + O(1)\,. \end{aligned} \tag{B.5}$$

The loop-function $\bar{G}(s)$ is discussed in Appendix C. We do not split the result into A_2, A_4, etc., because the propagators contain the physical pion mass at one-loop order – this would make the splitting rather useless.

B.2. $\gamma\gamma \to \pi^0\pi^0$

The leading term is generated by one-loop diagrams alone – there is no contribution from $\mathcal{L}_4$. The result is [1,2]

$$\begin{aligned} A_4 &= \frac{4(s - M^2)}{sF^2}\,\bar{G}(s)\,, \\ B_4 &= 0\,. \end{aligned} \tag{B.6}$$

CHPT thus predicts the cross section at this order in the energy expansion in terms of the two parameters F and M^2. The amplitude is purely S-wave.

In order to compare the prediction (B.6) with the data, we identify $F(M)$ with the physical pion decay constant F_π (physical pion mass M_π), as this induces only changes of higher order. The result is shown in Fig. 5, where we display the cross section $\sigma(s; |\cos\theta| \leqslant 0.8)$ according to Eq. (B.6) with a dashed line, together with the Crystal Ball data [9] as a function of the center-of-mass energy $E = \sqrt{s}$. The cross section is below the data for $E < 400$ MeV where the low-energy expansion can be trusted most. It also differs by a similar amount from dispersion theoretic calculations [10–16]. An example (Fig. 23 in Ref. [12]) is shown as dash-dotted lines in the figure. The solid line is the two-loop result.

The amplitude (B.6) has the peculiar property that its dispersive representation needs a subtraction, although the absorptive part vanishes at high energy sufficiently fast to generate a convergent unsubtracted dispersion integral,

$$\mathrm{Im}\, A = O\left(\frac{\ln s}{s}\right), \qquad s \to \infty. \tag{B.7}$$

Finally, we note that the leading term (B.6) approaches a constant in the chiral limit,

$$A(s) = -\frac{1}{4\pi^2 F^2} + O(E^2), \qquad \hat{m} \to 0, s \neq 0. \tag{B.8}$$

Appendix C. Loop-integrals

1. The loop-integral $\bar{G}(s)$ is

$$\bar{G}(s) = -\frac{1}{16\pi^2}\left\{1 + \frac{2M^2}{s}\int_0^1 \frac{dx}{x}\ln\left(1 - \frac{s}{M^2}x(1-x)\right)\right\}. \tag{C.1}$$

$\bar{G}$ is analytic in the complex s-plane, cut along the positive real axis for $\mathrm{Re}\, s \geqslant 4M^2$. At small s,

$$\bar{G}(s) = \frac{1}{16\pi^2}\sum_{n=1}^{\infty}\left(\frac{s}{M^2}\right)^n \frac{(n!)^2}{(n+1)(2n+1)!}. \tag{C.2}$$

The absorptive part is

$$\mathrm{Im}\,\bar{G}(s) = \frac{M^2}{8s\pi}\ln\left\{\frac{1+\sigma}{1-\sigma}\right\}, \qquad s > 4M^2,$$
$$\sigma = \sqrt{1 - 4M^2/s}. \tag{C.3}$$

Use of

$$\mathrm{Li}_2(y) + \mathrm{Li}_2\left(\frac{-y}{1-y}\right) = -\tfrac{1}{2}\ln^2(1-y),$$
$$\mathrm{Li}_2(y) = -\int_0^y \frac{dx}{x}\ln(1-x), \tag{C.4}$$

gives

$$-16\pi^2\bar{G}(s) = \begin{cases} 1 + \dfrac{M^2}{s}\left(\ln\dfrac{1-\sigma}{1+\sigma} + i\pi\right)^2; & 4M^2 \leqslant s, \\ 1 - \dfrac{4M^2}{s}\,\mathrm{arctg}^2\left(\dfrac{s}{4M^2-s}\right)^{1/2}; & 0 \leqslant s \leqslant 4M^2, \\ 1 + \dfrac{M^2}{s}\ln^2\dfrac{\sigma-1}{\sigma+1}; & s \leqslant 0. \end{cases} \tag{C.5}$$

In the text we also need

$$\bar{\bar{G}}(s) = \bar{G}(s) - s\bar{G}'(0). \tag{C.6}$$

2. The loop-integral $\bar{J}(s)$ is

$$\bar{J}(s) = -\frac{1}{16\pi^2}\int_0^1 \mathrm{d}x\,\ln\left(1 - \frac{s}{M^2}x(1-x)\right). \tag{C.7}$$

$\bar{J}$ is analytic in the complex s-plane, cut along the positive real axis for $\mathrm{Re}\,s \geqslant 4M^2$. At small s,

$$\bar{J}(s) = \frac{1}{16\pi^2}\sum_{n=1}^{\infty}\left(\frac{s}{M^2}\right)^n \frac{(n!)^2}{n(2n+1)!}. \tag{C.8}$$

The absorptive part is

$$\mathrm{Im}\,\bar{J}(s) = \frac{\sigma}{16\pi}, \qquad s > 4M^2. \tag{C.9}$$

Explicitly,

$$16\pi^2\bar{J}(s) = \begin{cases} \sigma\left(\ln\dfrac{1-\sigma}{1+\sigma} + i\pi\right) + 2; & 4M^2 \leqslant s, \\ 2 - 2\left(\dfrac{4M^2-s}{s}\right)^{1/2}\mathrm{arctg}\left(\dfrac{s}{4M^2-s}\right)^{1/2}; & 0 \leqslant s \leqslant 4M^2, \\ \sigma\ln\dfrac{\sigma-1}{\sigma+1} + 2; & s \leqslant 0. \end{cases} \tag{C.10}$$

In the text we also need

$$\bar{\bar{J}}(s) = \bar{J}(s) - s\bar{J}'(0). \tag{C.11}$$

3. The loop-function $\bar{H}$ is defined in terms of $\bar{G}$ and $\bar{J}$,

$$\bar{H}(s) = (s - 10M^2)\bar{J}(s) + 6M^2\bar{G}(s). \tag{C.12}$$

Appendix D. Low-energy constants from resonance saturation

Here we give details of the calculation needed to estimate the renormalized couplings a_1^r, a_2^r and b^r. We consider the exchange of scalar, (axial-)vector and tensor mesons with mass $M_R \leqslant 1.2$ GeV and follow the procedure outlined in Ref. [30]. The contributions of the vector and tensor mesons are evaluated in the framework of $SU(2)_L \times SU(2)_R \times U(1)$. In order to overcome the limitations about the experimental information presently available on the 1^{+-} and 0^{++} multiplets we will work in $SU(3)_L \times SU(3)_R$ at large N_C.

D.1. Vector and tensor mesons ($J^{PC} = 1^{--}, 2^{++}$)

D.1.1. The lagrangian

We set

$$V_\mu(1^{--}) \doteq \begin{cases} \frac{1}{\sqrt{2}} V_\mu^i \tau^i, & V = \rho, \\ \frac{1}{\sqrt{2}} V_\mu^0 \cdot \mathbf{1}, & V = \omega, \phi, \end{cases} \tag{D.1}$$

and have for the kinetic part

$$\mathcal{L}_{\text{kin}}(V,T) = -\tfrac{1}{4} \sum_V \langle V_{\mu\nu} V^{\mu\nu} - 2M_V^2 V_\mu V^\mu \rangle - \tfrac{1}{2} T_{\mu\nu} D^{\mu\nu;\rho\sigma} T_{\rho\sigma}, \tag{D.2}$$

where

$$\begin{aligned} V_{\mu\nu} &= D_\mu V_\nu - D_\nu V_\mu, \\ D_\mu V_\nu &= \partial_\mu V_\nu + [\Gamma_\mu, V_\nu], \\ \Gamma_\mu &= \tfrac{1}{2} \left\{ u^\dagger \left[\partial_\mu - i r_\mu \right] u + u \left[\partial_\mu - i l_\mu \right] u^\dagger \right\}. \end{aligned} \tag{D.3}$$

Furthermore, $T^{\mu\nu} = T^{\nu\mu}$ denotes the spin-2 field for $f_2(1270)$ with $J^{PC} = 2^{++}$, and

$$\begin{aligned} D^{\mu\nu;\rho\sigma} = (\Box + M_T^2) \left\{ \tfrac{1}{2} (g^{\mu\rho} g^{\nu\sigma} + g^{\nu\rho} g^{\mu\sigma}) - g^{\mu\nu} g^{\rho\sigma} \right\} \\ + g^{\rho\sigma} \partial^\mu \partial^\nu + g^{\mu\nu} \partial^\rho \partial^\sigma - \tfrac{1}{2} (g^{\nu\sigma} \partial^\mu \partial^\rho + g^{\nu\rho} \partial^\mu \partial^\sigma + g^{\mu\sigma} \partial^\nu \partial^\rho + g^{\mu\rho} \partial^\nu \partial^\sigma). \end{aligned} \tag{D.4}$$

The propagator for $T^{\mu\nu}$ is obtained in the standard manner by exposing the system to an external perturbation,

$$\mathcal{L} = \mathcal{L}_{\text{kin}}(T) + j^{\mu\nu} T_{\mu\nu}. \tag{D.5}$$

We find

$$G^{\mu\nu;\rho\sigma}(x) = (2\pi)^{-4} \int \frac{d^4p\ e^{-ipx}}{M_T^2 - p^2 - i\epsilon} P^{\mu\nu;\rho\sigma},$$
$$P_{\mu\nu;\rho\sigma} = \tfrac{1}{2}(P_{\mu\rho}P_{\nu\sigma} + P_{\mu\sigma}P_{\nu\rho}) - \tfrac{1}{3}P_{\mu\nu}P_{\rho\sigma},$$
$$P_{\mu\nu} = -g_{\mu\nu} + \frac{p_\mu p_\nu}{M_T^2}, \tag{D.6}$$

with

$$D^{\mu\nu;\rho\sigma}G_{\rho\sigma;}{}^{\alpha\beta}(x) = \tfrac{1}{2}(g^{\mu\alpha}g^{\nu\beta} + g^{\nu\alpha}g^{\mu\beta})\delta^4(x). \tag{D.7}$$

Now consider the couplings of V, T to pions and to photons, linear in the resonance fields. Since we are interested in terms of order E^6 in the effective action, it suffices to construct interactions which are at most of order E^3. We set $f_+^{\mu\nu} = 2eQF^{\mu\nu}$ where $F^{\mu\nu}$ is the photon field, and take

$$\mathcal{L}_{\rm int}(V,T) = e\epsilon_{\mu\nu\rho\sigma}F^{\mu\nu}\sum_V \{C_V^1\langle V^\rho\{u^\sigma, Q\}\rangle + C_V^2\langle V^\rho u^\sigma\rangle\langle Q\rangle\}$$
$$+ T_{\mu\nu}\{C_T^\pi\Theta_\pi^{\mu\nu} + e^2C_T^\gamma\Theta_\gamma^{\mu\nu}\}, \tag{D.8}$$

where $\Theta_\pi^{\mu\nu}$ ($\Theta_\gamma^{\mu\nu}$) is the energy–momentum tensor of the pion (photon) field,

$$\Theta_\pi^{\mu\nu} = \tfrac{1}{2}F^2\langle u^\mu u^\nu\rangle - \tfrac{1}{4}F^2g^{\mu\nu}\{\langle u^\sigma u_\sigma\rangle + \langle\chi_+\rangle\},$$
$$\Theta_\gamma^{\mu\nu} = F^\mu{}_\alpha F^{\alpha\nu} + \tfrac{1}{4}g^{\mu\nu}F^{\rho\sigma}F_{\rho\sigma}. \tag{D.9}$$

The coupling $V \to \pi\gamma$ ($T \to \pi\pi$, $\gamma\gamma$) has been considered in Ref. [52] (Ref. [25]) for the case of nonet fields and $\langle Q\rangle = 0$. The interaction (D.8) for the spin-2 field differs from the one proposed in Ref. [25]. In particular, our amplitude for $\gamma\gamma \to \pi^0\pi^0$ is smooth at large momenta and purely D-wave also off the f_2-resonance, see below.

D.1.2. The amplitudes

We find for the amplitudes from vector exchange

$$A_V = C_V\left[\frac{s - 4(t + M_\pi^2)}{M_V^2 - t} + \frac{s - 4(u + M_\pi^2)}{M_V^2 - u}\right],$$
$$B_V = \frac{C_V}{2}\left[\frac{1}{M_V^2 - t} + \frac{1}{M_V^2 - u}\right], \qquad V = \rho, \omega, \phi, \tag{D.10}$$

where [50,34,35,37,39]

$$C_V = \frac{3}{\alpha}M_V^3\frac{\Gamma(V \to \pi^0\gamma)}{(M_V^2 - M_\pi^2)^3}. \tag{D.11}$$

From the published [53] widths we obtain

$$C_\omega = 0.67\ \text{GeV}^{-2},$$
$$C_\rho = 0.12\ \text{GeV}^{-2},$$
$$C_\phi = 0.2 \times 10^{-2}\ \text{GeV}^{-2}. \tag{D.12}$$

The calculation of the ρ, ω correction to the $\gamma\gamma \to \pi^0\pi^0$ scattering amplitude has been extended recently to include both photons off shell [54].

Tensor exchange gives [10]

$$A_T + 2(4M_\pi^2 - s)B_T = 0,$$
$$B_T = \frac{1}{4}\frac{C_T^\gamma C_T^\pi}{M_T^2 - s}, \tag{D.13}$$

with

$$\Gamma(T \to \gamma\gamma) = \frac{(e^2 C_T^\gamma)^2 M_T^3}{80\pi},$$
$$\Gamma(T \to \pi^0\pi^0) = \frac{(C_T^\pi)^2 M_T^3}{960\pi}\left(1 - \frac{4M_\pi^2}{M_T^2}\right)^{5/2}. \tag{D.14}$$

From the measured widths $\Gamma(f_2 \to \gamma\gamma)$, $\Gamma(f_2 \to \pi^0\pi^0) = \frac{1}{3}\Gamma(f_2 \to \pi\pi)$ [53], we find

$$|C_T^\gamma| = 0.19\ \text{GeV}^{-1},$$
$$|C_T^\pi| = 9.2\ \text{GeV}^{-1}. \tag{D.15}$$

D.2. Axial-vector and scalar mesons ($J^{PC} = 1^{+-}, 0^{++}$)

D.2.1. The lagrangian

In this paragraph, $\bar{A}$ denotes a 3×3 matrix. In particular,

$$\bar{u}_\mu = -\frac{\partial_\mu \bar{\phi}}{F} + \dots,$$
$$\bar{\phi} = \sqrt{2}\begin{pmatrix} \frac{\pi^0}{\sqrt{2}} + \frac{\eta}{\sqrt{6}} & \pi^+ & K^+ \\ \pi^- & -\frac{\pi^0}{\sqrt{2}} + \frac{\eta}{\sqrt{6}} & K^0 \\ K^- & \bar{K}^0 & -\frac{2}{\sqrt{6}}\eta \end{pmatrix}, \tag{D.16}$$

and $\bar{Q} = \frac{1}{3}\,\text{diag}(2, -1, -1)$. (We do not include η–η' mixing, as this is of higher order in the quark mass expansion.) Furthermore, $\bar{B}_\mu$ stands for the axial-vector nonet,

$$\bar{B}_\mu(1^{+-}) = \frac{1}{\sqrt{2}} B_\mu^i \lambda^i + \frac{1}{\sqrt{3}} B_\mu^9 \cdot \mathbf{1}, \tag{D.17}$$

and similarly for the scalar nonet $\bar{S}(0^{++})$. The kinetic terms are

[10] The interaction (D.8) generates tadpole diagrams where T_ρ^ρ disappears in the vacuum. These graphs give rise to additional contributions to the amplitudes, which however are of higher order in the energy expansion. We omit them here.

$$\mathcal{L}_{\rm kin}(\bar{S},\bar{B}) = \tfrac{1}{2}\langle D^\mu \bar{S} D_\mu \bar{S} - M_S^2 \bar{S}^2\rangle - \tfrac{1}{4}\langle \bar{B}_{\mu\nu}\bar{B}^{\mu\nu} - 2M_B^2 \bar{B}_\mu \bar{B}^\mu\rangle\,, \tag{D.18}$$

where M_B denotes the common nonet mass, and the covariant derivatives are the $SU(3)$ version of (D.3). The couplings to pions and to photons are [30,25,38]

$$\begin{aligned}\mathcal{L}_{\rm int} = {} & e^2 C_S^\gamma F_{\mu\nu}F^{\mu\nu}\langle \bar{Q}^2\bar{S}\rangle + C_S^d\langle \bar{S}\bar{u}^\mu\bar{u}_\mu\rangle + C_S^m\langle \bar{S}\bar{\chi}_+\rangle \\ & + eC_B F_{\mu\nu}\langle \bar{B}^\mu\{\bar{Q},\bar{u}^\nu\}\rangle\,.\end{aligned} \tag{D.19}$$

D.2.2. The amplitudes

We find [11] for the contribution from the scalar exchange [25]

$$\begin{aligned}A_S &= \frac{20C_S^\gamma}{9F_\pi^2(M_S^2 - s)}\,[sC_S^d + 2M_\pi^2(C_S^m - C_S^d)]\,,\\ B_S &= 0\,,\end{aligned} \tag{D.20}$$

with

$$\Gamma(a_0 \to \gamma\gamma) = \frac{(e^2C_S^\gamma)^2 M_S^3}{72\pi}\,. \tag{D.21}$$

The couplings C_S^d and C_S^m have been determined in Ref. [30],

$$\begin{aligned}|C_S^d| &= 3.2\times 10^{-2}\ \text{GeV}\,,\\ |C_S^m| &= 4.2\times 10^{-2}\ \text{GeV}\,,\\ C_S^dC_S^m &> 0\,.\end{aligned} \tag{D.22}$$

The quantity $|C_S^\gamma|$ is difficult to estimate. Here we content ourselves with a rough estimate by relating it to the decay $a_0 \to \gamma\gamma$ via

$$\Gamma(a_0 \to \gamma\gamma) = r\,\frac{\Gamma_{\rm tot}}{\Gamma(a_0 \to \pi^0\eta)}\,, \tag{D.23}$$

where $r = 0.24$ keV [53] with a sizeable error. We furthermore assume that the decay $a_0 \to \pi^0\eta$ accounts for all of $\Gamma_{\rm tot}$,

$$\Gamma_{\rm tot} = \Gamma(a_0 \to \pi^0\eta)\,. \tag{D.24}$$

Hence we obtain

$$|C_S^\gamma| = 8.2\times 10^{-2}\ \text{GeV}^{-1}\,. \tag{D.25}$$

For the contribution from the axial nonet exchange [50,38] we find

[11] The interaction (D.19) generates tadpole diagrams where $\langle\bar{S}\rangle$ disappears in the vacuum. These graphs give rise to additional contributions to the amplitudes, which however are of higher order in the energy expansion. We omit them here.

$$A_B = C_B \left[\frac{s + 4(t - M_\pi^2)}{M_B^2 - t} + \frac{s + 4(u - M_\pi^2)}{M_B^2 - u} \right],$$

$$B_B = \frac{C_B}{2} \left[\frac{1}{M_B^2 - t} + \frac{1}{M_B^2 - u} \right] \tag{D.26}$$

with

$$C_B = \frac{30}{\alpha} M_B^3 \frac{\Gamma(b_1 \to \pi^+ \gamma)}{(M_B^2 - M_\pi^2)^3} \tag{D.27}$$

or

$$C_B = 0.53 \text{ GeV}^{-2}. \tag{D.28}$$

D.3. Expressions at low energies

At low energies, the above contributions from V, B, S and T sum up to

$$A_6 = \bar{a}_1 M_\pi^2 + \bar{a}_2 s,$$

$$B_6 = \bar{b},$$

$$\bar{a}_1 = -16 \sum_{V=\rho,\omega,\phi} \frac{C_V}{M_V^2} \pm \left(\frac{40}{9} \frac{|C_S^\gamma (C_S^m - C_S^d)|}{F_\pi^2 M_S^2} - 2 \frac{|C_T^\gamma C_T^\pi|}{M_T^2} \right),$$

$$\bar{a}_2 = 6 \sum_{V=\rho,\omega,\phi} \frac{C_V}{M_V^2} - 2 \frac{C_B}{M_B^2} \pm \left(\frac{20}{9} \frac{|C_S^\gamma C_S^d|}{F_\pi^2 M_S^2} + \frac{1}{2} \frac{|C_T^\gamma C_T^\pi|}{M_T^2} \right),$$

$$\bar{b} = \sum_{V=\rho,\omega,\phi} \frac{C_V}{M_V^2} + \frac{C_B}{M_B^2} \pm \frac{1}{4} \frac{|C_T^\gamma C_T^\pi|}{M_T^2}. \tag{D.29}$$

In Table 2 we list the contributions from the individual resonances to the dimensionless parameters $(16\pi^2 F_\pi^2)^2 (\bar{a}_1; \bar{a}_2; \bar{b})$. We used the following values for the resonance masses: $M_\omega = 782$ MeV, $M_\rho = 768$ MeV, $M_\phi = 1020$ MeV, $M_B = 1232$ MeV, $M_S = 983$ MeV, $M_T = 1275$ MeV.

References

[1] J. Bijnens and F. Cornet, Nucl. Phys. B 296 (1988) 557.
[2] J.F. Donoghue, B.R. Holstein and Y.C. Lin, Phys. Rev. D 37 (1988) 2423.
[3] S. Weinberg, Physica A 96 (1979) 327.
[4] J. Gasser and H. Leutwyler, Ann. Phys. (N.Y.) 158 (1984) 142.
[5] J. Gasser and H. Leutwyler, Nucl. Phys. B 250 (1985) 465.
[6] H. Leutwyler, Bern University, preprint BUTP-93/24 (hep-ph/9311274), Ann. Phys. (N.Y.), in print.
[7] For recent reviews on CHPT see e.g. H. Leutwyler, *in* Proc. XXVI Int. Conf. on High Energy Physics, Dallas, 1992, ed. J.R. Sanford, AIP Conf. Proc. No. 272 (AIP, New York, 1993) p. 185;
U.G. Meißner, Rep. Prog. Phys. 56 (1993) 903;
A. Pich, Lectures given at the V Mexican School of Particles and Fields, Guanajuato, México, December 1992, preprint CERN-Th.6978/93 (hep-ph/9308351);

G. Ecker, Lectures given at the 6th Indian-Summer School on Intermediate energy physics interaction in hadronic systems, Prague, August 25–31, 1993, to appear in the Proc. (Czech. J. Phys.), preprint UWThPh -1993-31 (hep-ph/9309268).
[8] Mark II Collab., J. Boyer et al., Phys. Rev. D 42 (1990) 1350.
[9] Crystal Ball Collab., H. Marsiske et al., Phys. Rev. D 41 (1990) 3324.
[10] R.L. Goble, R. Rosenfeld and J.L. Rosner, Phys. Rev. D 39 (1989) 3264. The literature on earlier work may be traced from this reference.
[11] D. Morgan and M.R. Pennington, Phys. Lett. B 272 (1991) 134.
[12] M.R. Pennington, in Ref. [18], p. 379.
[13] J.F. Donoghue and B.R. Holstein, Phys. Rev. D 48 (1993) 137.
[14] A. Dobado and J.R. Peláez, Z. Phys. C 57 (1993) 501.
[15] T.N. Truong, Phys. Lett. B 313 (1993) 221.
[16] A.E. Kaloshin and V.V. Serebryakov, Irkutsk preprint ISU-IAP.Th93-03 (hep-ph/9306224).
[17] G. Pancheri, ed., Proc. Workshop on Physics and Detectors for DAΦNE, Frascati, 1991 (INFN, Frascati, 1991).
[18] L. Maiani, G. Pancheri and N. Paver, eds., The DAΦNE Physics Handbook (INFN, Frascati, 1992).
[19] T.N. Truong, Phys. Rev. Lett. 61 (1988) 2526.
[20] S. Weinberg, Phys. Rev. Lett. 17 (1966) 616.
[21] J. Gasser and U.G. Meißner, Nucl. Phys. B 357 (1991) 90.
[22] N.H. Fuchs, H. Sazdjian and J. Stern, Phys. Lett. B 269 (1991) 183.
[23] M. Knecht, B. Moussallam and J. Stern, preprint IPNO/TH 94-08 (hep-ph/9402318).
[24] J. Wess and B. Zumino, Phys. Lett. B 37 (1971) 95;
E. Witten, Nucl. Phys. B 223 (1983) 422;
N.K. Pak and P. Rossi, Nucl. Phys. B 250 (1985) 279.
[25] Ll. Ametller, J. Bijnens, A. Bramon and F. Cornet, Phys. Lett. B 276 (1992) 185.
[26] J. Bijnens et al., work in progress.
[27] J.C. Collins, Renormalization (Cambridge University Press, Cambridge, 1984).
[28] G. 't Hooft, Nucl. Phys. B 61 (1973) 455;
S. Weinberg, Phys. Rev. D 8 (1973) 3497;
J.C. Collins, Nucl. Phys. B 80 (1974) 341.
[29] W.A. Bardeen, A.J. Buras, D.W. Duke and T. Muta, Phys. Rev. D 18 (1978) 3998.
[30] G. Ecker, J. Gasser, A. Pich and E. de Rafael, Nucl. Phys. B 321 (1989) 311;
G. Ecker et al., Phys. Lett. B 223 (1989) 425;
J.F. Donoghue, C. Ramirez and G. Valencia, Phys. Rev. D 39 (1989) 1947;
M. Praszalowicz and G. Valencia, Nucl. Phys. B 341 (1990) 27;
J. Bijnens, S. Dawson and G. Valencia, Phys. Rev. D 44 (1991) 3555;
Ll. Ametller, J. Bijnens, A. Bramon and F. Cornet, Ref. [25].
[31] J. Bijnens, G. Ecker and J. Gasser, in Ref. [18], p. 107.
[32] A. Schenk, Nucl. Phys. B 363 (1991) 97.
[33] J. Stern, H. Sazdjian and N.H. Fuchs, Phys. Rev. D 47 (1993) 3814.
[34] P. Ko, Phys. Rev. D 41 (1990) 1531.
[35] J. Bijnens, S. Dawson and G. Valencia, Ref. [30].
[36] S. Bellucci and D. Babusci, in Ref. [17], p. 351.
[37] S. Bellucci, in Ref. [18], p. 419.
[38] P. Ko, Phys. Rev. D 47 (1993) 3933.
[39] D. Babusci, S. Bellucci, G. Giordano and G. Matone, Phys. Lett. B 314 (1993) 112.
[40] For reviews on polarizabilities see e.g.
V.A. Petrunkin, Sov. J. Part. Nucl. 12 (1981) 278;
J.L. Friar, *in* Proc. Workshop on Electron–Nucleus Scattering, Marciana Marina, 7–15 June 1988, eds. A. Fabrocini et al. (World Scientific, Singapore, 1989) p. 3;
B.R. Holstein, Comm. Nucl. Part. Phys. 19 (1990) 221;
M.A. Moinester, *in* Proc. 4th Conf. on the Intersections Between Particle and Nuclear Physics, Tucson, Arizona, May 24–29, 1991, AIP Conf. Proc. No. 243, ed. W.T.H. Van Oers (AIP, New York, 1992), p. 553.

[41] Yu.M. Antipov et al., Phys. Lett. B 121 (1983) 445; Z. Phys. C 24 (1984) 39.
[42] T.A. Aibergenov et al., Czech. J. Phys. B 36 (1986) 948.
[43] Yu.M. Antipov et al., Z. Phys. C 26 (1985) 495.
[44] A.E. Kaloshin and V.V. Serebryakov, Phys. Lett. B 278 (1992) 198.
[45] J.F. Donoghue, J. Gasser and H. Leutwyler, Nucl. Phys. B 343 (1990) 341.
[46] V.B. Golubev et al., Sov. J. Nucl. Phys. 45 (1987) 622.
[47] D. Babusci et al., in Ref. [17], p. 383; Phys. Lett. B 277 (1992) 158.
[48] J. Gasser, talk given at the EURODAFNE Workshop (Frascati, April 1993).
[49] U. Bürgi, work in progress.
[50] A.E. Kaloshin and V.V. Serebryakov, Z. Phys. C 32 (1986) 279.
[51] J.F. Donoghue, private communication;
J. Kambor and B.R. Holstein, Phys. Rev. D 49 (1994) 2346.
[52] G. Ecker, A. Pich and E. de Rafael, Phys. Lett. B 237 (1990) 481.
[53] Particle Data Group, K. Hikasa et al., Phys. Rev. D 45 (1992) S1.
[54] S. Bellucci and G. Colangelo, Phys. Rev. D 49 (1994) 1207.
[55] R.J. Eden, P.V. Landshoff, D.I. Olive and J.C. Polkinghorne, The analytic S-matrix (Cambridge Univ. Press, Cambridge, 1966).